İSTANBUL TECHNICAL UNIVERSITY ★ INSTITUTE OF SCIENCE AND TECHNOLOGY

DETECTION OF REFLECTION COEFFICIENT CHARACTERISTICS WITH DIFFERENT ANTENNA ORIENTATION BY GROUND PENETRATING RADAR

M.Sc. Thesis by

Musavver Didem SAMUT, B.Sc.

Department : Geophysical Engineering

Programme: Geophysical Engineering

MAY 2003

İSTANBUL TECHNICAL UNIVERSITY ★ INSTITUTE OF SCIENCE AND TECHNOLOGY

DETECTION OF REFLECTION COEFFICIENT CHARACTERISTICS WITH DIFFERENT ANTENNA ORIENTATION BY GROUND PENETRATING RADAR

M.Sc. Thesis by

Musavver Didem SAMUT, B.Sc.

(505011185)

Date of submission : 5 May 2003

Date of defence examination: 29 May 2003

Supervisor (Chairman): Assoc. Prof. Dr. Berkan ECEVİTOĞLU

Members of the Examining Committee Assoc. Prof. Dr. Emin DEMİRBAĞ (İTÜ.)

Ass. Prof. Dr. Hüseyin TUR (İÜ.)

MAY 2003

PREFACE

This thesis contains a part of Interurban Project of Berlin Technical University, which clarifies the dynamics of water and materials at urban locations. In order to map the water distribution in the selected field, Ground Penetrating Radar measurements have been performed with a number of other geophysical methods. These GPR measurements constitute the infrastructure of my thesis with a deep theoretical background.

After taking all the difficulties in performing master education, diploma thesis is the last step for graduation. This thesis was performed with the help of some important people. I would like to thank to my supervisor Assoc. Prof. Dr. Berkan Ecevitoglu who encouraged during my studies. I want to thank to him for his helpful advices and fruitful contribution to this thesis. I would like to acknowledge to Prof Dr. Ugur Yaramancı who gave me the opportunity to perform this present thesis with the technical support of Berlin Technical University. He gave me the idea of this subject for my thesis. I would like to thank to my colleague, Juergen Schmalholz who contributed during my studies from beginning till the end. I would like to thank to my friend Caner Cambaz for his morale support during my studies. I am especially grateful to my family, who supported my studies not only in this work, but also in whole of my life period.

May 2003 M. Didem SAMUT

CONTENTS

ABBREVIATIONS

CMP	: Common Mid Point
EM	: Electromagnetic
FD	: Finite Difference
GPR	: Ground Penetrating Radar
RADAR	: Radio Detection and Ranging
SIP	: Spectral Induced Polarization
SNMR	: Surface Nuclear Magnetic Resonance
TE	: Transient Electric
TM	: Transient Magnetic

LIST OF TABLES

LIST OF FIGURES

SYMBOLS

E	: Electric field intensity vector
B	: Magnetic induction vector
H	: Magnetic field intensity vector
D	: Electric displacement vector
J	: Current density vector
α	: Attenuation factor
β	: Phase factor
c	: Electromagnetic wave velocity
ε	: Dielectric permittivity
ε_0	: Dielectric permittivity of the free space
ε_r	: Relative dielectric permittivity
δ	: Skin depth
k	: Complex wave number
ρ	: Electric charge density
μ	: Magnetic permeability
μ_0	: Magnetic permeability of the free space
μ_r	: Relative magnetic permeability
σ	: Electrical conductivity
t	: Time
ω	: Angular frequency
E_0	: Amplitude of the electric field

P	**:** Loss factor
	:

YERALTI RADARINDA YANSIMA SAYISI KARAKTERİNİN DEĞİŞİK ANTEN YÖNELİMİ İLE BELİRLENMESİ

ÖZET

30 yılı aşkın bir süredir yeraltı radarı jeofizik uygulamalarında kullanılmaktadır. Özellikle çevresel, mühendislik ve arkeolojik çalışmalarda olmak üzere çok kullanım alanı vardır. Bu çalışmada farklı anten yönelimlerinde yansıma katsayısı karakterini belirlemek için yeraltı radarı ölçümleri yapılmıştır. Düzlemsel arayüzeyde elektromanyetik dalganın davranışı Snell yasası ve Fresnel Denklemleri kullanılarak açıklanabilir. Brewster açısının geliştirilmesiyle ortak orta nokta (CMP) ölçülerinden ara yüzeydeki iki ortamın dielektrik permittivite oranları belirlenebilir. Bu bilgi özellikleri bilinmeyen ikinci ortamın belirlenmesinde kullanılabilir. Bu çalışmanın asıl amacı elektrik alanın yansıma düzlemine dik ve paralel olduğu iki anten yönelimi üzerine odaklanmaktır. Bu amaçla, arazi çalışmasını gerçekleştirmek için Tiergarten - Berlin'de iyi bilinen bir test alanı seçilmiştir. Profil yönüne paralel ve dik anten yönelimleri için değişken ve sabit ofset ölçümleri kullanılarak 50, 100, 200, 400 MHz anten frekansları kullanılmıştır. Seçilen test sahasında 150'den fazla ölçü alınmıştır. Bütün veriler işlenmiş, yorumlanmış ve diğer yönelimler ile karşılaştırılmıştır. Arazi karakterinin ölçülen veri ile karşılaştırılması için arazi modelleri, yansıma katsayısı karakteri ve anten karakteri de bu çalışmada tartışılmıştır. Ortaya çıkan yeraltı radarı kesitleri anten yönelimine gore değişen sonuçlar vermektedir. Sonuçlar yer altı radarı verisinin anten yönüne bağımlı olduğunu göstermektedir. Yer altı radarı ölçmelerinde değişik anten yönelimlerinin kullanılması daha güvenilir sonuçlar sağlar. CMP ölçülerinde Brewster açısının belirlenmesi yeraltı yapısının özelliklerinden dolayı mümkün olmamıştır.

DETECTION OF REFLECTION COEFFICIENT CHARACTERISTICS WITH DIFFERENT ANTENNA ORIENTATION BY GROUND PENETRATING RADAR

SUMMARY

Ground Penetrating Radar (GPR) is used for more than 30 years in geophysical applications. It has a wide variety of application fields especially in environmental, engineering and archeological studies. In this study, GPR measurements were performed to determine the reflection coefficient characteristics for different antenna orientations. Electromagnetic wave behavior at a plane interface can be described by using the *Snell's law* and the *Fresnel equations*. By utilizing the Brewster Angle, dielectric permittivity ratios of two media at an interface can be determined from common midpoint (CMP) measurements. This information can be used to identify the unknown second media. The main aim of this work is to focus on two antenna orientations with the electric field, perpendicular and parallel to the plane of incidence. For this purpose, a well known test field in Tiergarten, Berlin was selected to perform the field work. Parallel and perpendicular antenna orientations to the profiling direction were used with variable offset and constant offset measurements using 50, 100, 200, 400 MHz antenna frequencies. More than 150 profiles were carried out at the selected field. All the data have been processed, interpreted and then compared with other orientations. Forward models of the field, reflection coefficient characteristics and antenna characteristics have been also discussed in this study to compare the field characteristics with the measured data The resultant sections of the GPR measurements give different results depending on the antenna orientation. The results show that ground penetrating radar data is dependent on antenna orientation. Use of various orientation in ground penetrating radar measurements provide more reliable results. Detection of the Brewster angle was not possible in CMP measurements because of the subsurface structure characteristics.

1. INTRODUCTION

Ground Penetrating Radar (GPR) is used for more than 30 years in geophysical applications. It provides a quick and easy way to image the shallow subsurface with a relative good resolution. It is an electromagnetic technique that uses electromagnetic waves in the frequency band of 10-1000 MHz. The advantage of using EM waves is that signals relatively short wavelength can be generated and radiated into the ground to detect anomalous variations in the dielectric properties of the geological material. GPR waves respond to changes in dielectrical contrasts in soils and rocks associated with geological conditions such as water intrusion, clay content, humidity, voids, fractures, bedding and buried objects.

Radar in geophysics has a wide variety of application fields especially in environmental and engineering problems. Some of the application fields are environmental site characterization, and monitoring, locating lost utilities, agriculture and archeological surveys. Road, runways, pavements, forensic and geothecnical studies, grave location, groundwater, infrastructure, ice, permafrost, sinkholes, tunnel and void detection can be the most popular examples of radar application. It's being a non-destructive method makes it suitable for use in urban settings and archeological environments.

GPR methodology is similar to the seismic reflection techniques. Both of the methods use reflection of energy from underground structures. But they are quite different in many respects. GPR cannot penetrate into materials of high electrical conductivity such as damp clays. But they are excellent targets for the seismic reflection technique. On the other hand radar penetrates dry sand and gravel that will not easily transmit high-frequency seismic waves. It is most effective in low attenuation media such as ice, sand, fresh water etc. and less effective or even ineffective in high attenuation media such as wet clay, wet silt, salt water etc.

A variety of survey design can be used in GPR measurements. Constant offset measurements identify the reflector lithology by imaging the subsurface. Variable offset measurements are used to obtain the radar signal velocity versus depth. The velocity structure can be obtained by varying the antenna offset at a fixed location.

In this present work GPR measurements were performed to determine the reflection coefficient characteristics with different antenna orientations. Electromagnetic wave behavior at a plane interface can be described by using the *Snell's law* and the *Fresnel equations*. Snell's law describes the angular relations between the propagation vectors. Fresnel equations describe the amplitude relation of the reflected and incident wave of an electric and magnetic field. The aim of this work is to present the investigation of reflection coefficient characteristics with different antenna orientation at a test field above the ground water table. The main orientations used in this work are the ones with the electric field, perpendicular and parallel to the plane of incidence. Brewster Angle can be detected with antenna orientation that the electric field is parallel to the plane of incidence. Utilizing the Brewster Angle, dielectric permittivity ratios of two media at an interface can be determined on CMP measurements. For this purpose, a well-known test field in Tiergarten, Berlin was selected to perform the field measurements. Parallel and perpendicular antenna orientations to the profiling direction have been used for variable offset and constant offset measurements by using 50, 100, 200, 400 MHz antenna frequencies. More than 150 profiles were carried out at the selected field. All the data have been processed, interpreted and then compared with other orientations. Second chapter of this work gives information about the theory and derivation of the electromagnetic wave equations. Electromagnetic wave behavior at an interface was presented in detail. Brief information about the characteristics of the test site will be given in the third chapter. In the fourth chapter field measurements will be presented. Methodology, data processing and results of the measurements will take place in this chapter for constant offset and variable offset measurements. Fifth chapter discusses reflection characteristics from ground water. Forward models of the field data reflection and antenna characteristics will be discussed in the same chapter. And finally, last chapter will summarize and conclude this present work.

2. THEORETICAL BASIS

2.1. Propagation of Electromagnetic Waves

GPR waves propagate at high frequencies in the range of 10 – 1000 MHz. In these frequency range electromagnetic waves obey Maxwell's equations in a linear, homogeneous and isotropic medium. Maxwell's equations describe the propagation of an electromagnetic wave in a layer by using the parameters E, B, H, J and D in the time domain.

$$\nabla\times \mathrm{E} = -\frac{\partial B}{\partial t} \qquad (2.1)$$

$$\nabla\times \mathrm{H} = \mathrm{J} + \frac{\partial D}{\partial t} \qquad (2.2)$$

$$\nabla.\mathrm{B} = 0 \qquad (2.3)$$

$$\nabla.\mathrm{D} = \rho \qquad (2.4)$$

where, E is the electric field intensity (V/m), B is the magnetic induction (Wb/m^2 or Tesla), D is the dielectric displacement (C/m^2), H is the magnetic field intensity (A/m), J is the electric current density (A/m^2), ρ is the electric charge density (c/m^3) and t is time (s). However there is no relationship of the electromagnetic field to the subsurface structure of the earth. Constitutive equations describe the relationship between these equations and the subsurface structure of the earth. Derivations of Maxwell's equations and constitutive relations have been discussed in detail at Stratton [1] and Ward et. al. [2]

$$\mathrm{J}=\sigma\mathrm{E} \qquad (2.5)$$

$$D=\varepsilon E \quad (2.6)$$

$$B=\mu H \quad (2.7)$$

In which the tensors, σ, ε, μ describe respectively the electric conductivity (S/m), dielectric permittivity (F/m) and the magnetic permeability (H/m) in the frequency domain, where

$$\varepsilon=\varepsilon_0 \varepsilon_r \quad (2.8)$$

$$\mu=\mu_0 \mu_r \quad (2.9)$$

ε_r is the relative dielectric permittivity or dielectric constant, ε_0 is the dielectric permittivity of the free space (= 8,854 x 10^{-12} F/m), μ_r is the relative magnetic permeability, μ_0 is the magnetic permeability of the free space (= 4π x 10^{-7} H/m) in Eq. (2.8) and Eq. (2.9). The relative magnetic permeability value is accepted as 1 for most of the materials. Relative magnetic permeability values for some of the minerals are presented at Table 2.1 from Telford et.al [3].

Table 2.1. Relative magnetic permeabilities of some minerals from Telford et. al. [3]

Mineral	Permeability
Magnetite	5
Pyrrhotite	2.55
Hematite	1.05
Pyrite	1.0015
Rutile	1.0000035
Calcite	0.999987
Quartz	0.999985

By using Maxwell’s equations and constitutive relationships it is possible to reduce Maxwell’s equations in terms of two parameters, E and H. When one-dimensional (1-D) Fourier transformation applied to Eq. (2.1) and Eq. (2.2) it is possible to obtain Maxwell’s equations in the frequency domain

$$\nabla\times E + i\mu\omega H = 0 \tag{2.10}$$

$$\nabla\times H - (\sigma + i\omega\varepsilon)E = 0 \tag{2.11}$$

Taking the curl of each equation and by substituting the constitutive equations, they become

$$\nabla \times \nabla \times E + \mu \nabla \times \frac{\partial H}{\partial t} = 0 \tag{2.12}$$

$$\nabla \times \nabla \times H - \varepsilon \nabla \times \frac{\partial E}{\partial t} = \sigma \nabla \times E \tag{2.13}$$

The vector identity can be used to utilize these equations

$$\nabla\times\nabla\times a = \nabla\nabla.a - \nabla^2 a \tag{2.14}$$

$$\nabla^2 E - \mu\varepsilon \frac{\partial^2 E}{\partial t^2} - \mu\sigma \frac{\partial E}{\partial t} = 0 \tag{2.15}$$

$$\nabla^2 H - \mu\varepsilon \frac{\partial^2 H}{\partial t^2} - \mu\sigma \frac{\partial H}{\partial t} = 0 \tag{2.16}$$

After this, Eq. (2.15) and Eq. (2.16) states the wave equations for the electric and magnetic field in time domain. Utilizing the Fourier Transformation of these equations with respect to time leads to

$$\nabla^2 E + (\mu\varepsilon\omega^2 - i\mu\sigma\omega)E = 0 \tag{2.17}$$

$$\nabla^2 H + (\mu\varepsilon\omega^2 - i\mu\sigma\omega)H = 0 \tag{2.18}$$

and

$$\nabla^2 E + k^2 E = 0 \tag{2.19}$$

$$\nabla^2 H + k^2 \ H = 0 \tag{2.20}$$

In these equations μ, ε and σ are the physical parameters of the earth as functions of frequency. These rock properties can be grouped into one term, given by

$$k^2 = \varepsilon\mu\omega^2 - i\mu\sigma\omega \tag{2.21}$$

In Eq. (2.21) the quantity k is called the complex wave number. The behavior of this parameter with change of frequency is important to understand the electromagnetic wave propagation and attenuation.

If the frequency is in the range of 10 MHz or higher, such as radar waves, displacement currents dominate over conduction currents ($\varepsilon\mu\omega^2 >> i\mu\sigma\omega$) (this statement also means small conductivity values in the field. For this case complex wave number can be defined as $k^2 = \mu\varepsilon\omega^2$. In such a regime of high frequency conductivity and low conductivity, the propagation of the EM waves depends mainly on the dielectric constant of the rock.

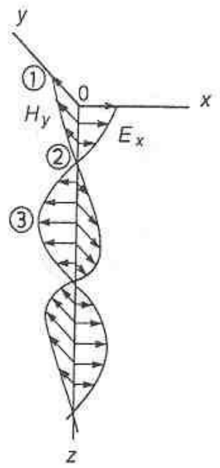

Figure 2.1. The sinusoidal behavior of the electric field (Ex) and magnetic field (Hy) as functions of time and propagation distance z. [4]

In the case of a plane wave, if the wave propagates in the z-direction (vertically downwards) with an electric field having only an x-component and the magnetic field only a y-component, amplitudes of these two fields vary sinusoidally with z as in Fig. 2.1 from Sharma [4]. For this case, Eq. (2.17) and Eq. (2.18) have a simple solution, given by

$$E = E_0 e^{i(\omega t - kz)} \tag{2.22}$$

E_0 is the amplitude of the electric field component at some point in the medium, for instance (z=0). k is the complex wave number. Since k is complex, it can be defined as;

$$k = \alpha \pm i\beta \tag{2.23}$$

The real part of *k* is associated with the phase factor, β (rad/m), and the imaginary part is associated with the attenuation factor, α (db/m), of the wave. The expressions for the phase and attenuation factors, respectively, are

$$\beta = \omega \left[\left(\frac{\mu\varepsilon}{2} \right) \left(\left[1 + \left(\frac{\sigma}{\varepsilon\omega} \right)^2 \right]^{1/2} - 1 \right) \right]^{1/2} \tag{2.24}$$

$$\alpha = \omega \left[\left(\frac{\mu\varepsilon}{2} \right) \left(\left[1 + \left(\frac{\sigma}{\varepsilon\omega} \right)^2 \right]^{1/2} + 1 \right) \right]^{1/2} \tag{2.25}$$

In these two equations, Eq. (2.24) and (2.25), the parameters in the inner part of the equations can be defined with a new parameter P, called loss factor.

$$P = \frac{\sigma}{\varepsilon\omega} \tag{2.26}$$

If we rewrite the Eq. (2.22) physical meaning of the parameters α and β can be easily understood.

$$E = E_0 e^{-\alpha z} e^{i(\beta z - \omega t)} \tag{2.27}$$

The real part of the wave number, k, attenuate exponentially in z direction. The term skin depth can be described as the attenuative characteristics of the medium in terms of the distance δ, over which the field strength is reduced by the factor 1/e.

$$\delta = \frac{1}{\alpha} = \left(\frac{2}{\sigma}\right)\left(\frac{\varepsilon}{\mu o}\right) \qquad (2.28)$$

In low loss materials, P≈0, velocity can be described as

$$v = c / (\mu_r \varepsilon_r)^{1/2} \qquad (2.29)$$

where c is the speed of light in free space. As it is already known that the value of the parameter μ_r is accepted as 1 for most of the geological materials. Thus, radar wave velocity is primarily controlled by the relative dielectric permittivity, ε_r, of the medium [5].

Table 2.2. Table of relative dielectric permittivity, electrical conductivity, velocity and attenuation values observed in common geological materials at 100 MHz from Davis and Annan [6]

Material	ε_r	σ (mS/m)	v (m/ns)	α (db / m)
Air	1	0	0,30	0
Distilled water	80	0,01	0,033	2×10^{-3}
Fresh water	80	0,5	0,033	0,1
Sea water	80	3×10^4	0,01	10^3
Dry sand	3 - 5	0,01	0,15	0,01
Saturated sand	20 - 30	0,1 – 1,0	0,06	0,03 – 0,3
Limestone	4 - 8	0,5 - 2	0,12	0,4 - 1
Shale	5 - 15	1 - 100	0,09	1 - 100
Silts	5 - 30	1 - 100	0,07	1 - 100
Clays	5 - 40	2 – 1000	0,06	1 - 300
Granite	4 - 6	0,01 - 1	0,13	0,01 - 1
Dry salt	5 - 6	0,01 - 1	0,13	0,01 - 1
Ice	3 - 4	0.01	0.16	0.01

Table 2.2 represents the relative dielectric permittivity, electrical conductivity, velocity, and attenuation values observed in common geological materials at 100 MHz. The velocity and the attenuation are the factors that describe the propagation of high frequency radio waves in the ground. The attenuation depends both upon the conductivity and the dielectric permittivity of the subsurface. But these two parameters are not the only one that effects attenuation of radar waves. Frequency is one of the other parameter that effects the attenuation. The most important parameter in radar wave

velocity is the dielectric permittivity of the material. In most geological environments water will cause the principal contrast in dielectric permittivity and hence, the bulk dielectric constant of the medium will be measure of the moisture content [7]. Most of the minerals have a relative dielectric permittivity values in the range of 5-7. But the relative dielectric permittivity of water is about 80. This large difference explains why the radar signal velocity is strongly dependent on the water content in soils. Based upon the Eq. (2.29) the electromagnetic wave velocity is essentially a measure of the water content, which is also a measure of the porosity.

2.2. Reflection Coefficient Characteristics At An Interface

Electromagnetic wave behavior at a plane interface can be described by using the Snell's law and the Fresnel equations. Snell's law describes the angular relationships between the propagation vectors. Fresnel equations describe the amplitude relation of the reflected and incident wave of an electric and magnetic field. Reflection, R, and Transmission, T, coefficients are simple functions of relative dielectric permittivity. When EM waves are obliquely incident on an interface between two media, two different cases must be considered. In the first case, electric field vector is perpendicular to the plane of incidence. This can be referred to as 'Transient Electric Mode' (TE Mode) or perpendicular polarization. In this case the incident ray is in the plane of incidence and it's normal to the surface. In the second case the electric field vector is parallel to the plane of incidence. This can is referred to as 'Transient Magnetic Mode' (TM Mode) or parallel polarization. TE and TM modes are more analogous to SH and SV waves in seismic, respectively.

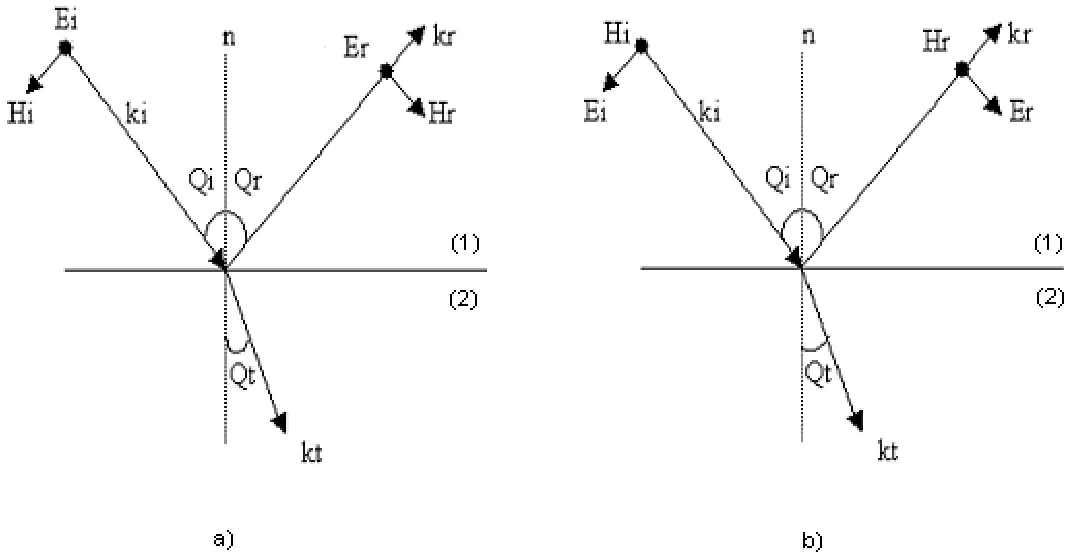

Figure 2.2. Relative orientations of the E, H and k vectors for reflection at a plane interface. a) E is normal to the plane of incidence (TE Mode). b) H is normal to the plane of incidence (TM Mode).

Figure 2.2 represents the reflection of electric and magnetic field vectors from an interface for two different antenna orientations. (1) and (2) represent two different layers of an interface with different electrical properties. ε_1, μ_1, σ_1 are the electrical properties of the first layer and, ε_2, μ_2, σ_2 are for the second layer. In TE mode E, H and k vectors are orthogonal to each other and the E field is normal to the plane of incidence. In the second case with TM mode three vectors are orthogonal to each other but the H field is normal to the plane of incidence.

Polarization type effects how the wave is reflected from a planar surface or a buried object. In the perpendicular polarization the ratio of the reflected to the incident electric field is termed the amplitude reflection coefficient, $r_\perp$, for Ei perpendicular to the plane of incidence. The symbol $r_\perp$ can be also represented by $\mathbf{r}_{TE}$ to indicate that the reflection coefficient applied to waves transverse electric to z.

$$r_\perp \equiv \frac{Er}{Ei} = \frac{\mu 2\, k1 \cos Qi - \mu 1\, k2 \cos Qt}{\mu 2\, k1 \cos Qi + \mu 1\, k2 \cos Qt} \qquad (2.30)$$

In the parallel polarization the magnetic vector must be normal to the plane of incidence, so that

$$r_{||} \equiv \frac{Hr}{Hi} = \frac{\mu 1\, k2 \cos Qi - \mu 2\, k1 \cos Qt}{\mu 1\, k2 \cos Qi + \mu 2\, k1 \cos Qt} \qquad (2.31)$$

The symbol r|| can be represented by $\mathbf{r}_{TM}$ to indicate that the reflection coefficient applied to waves transverse magnetic to z.

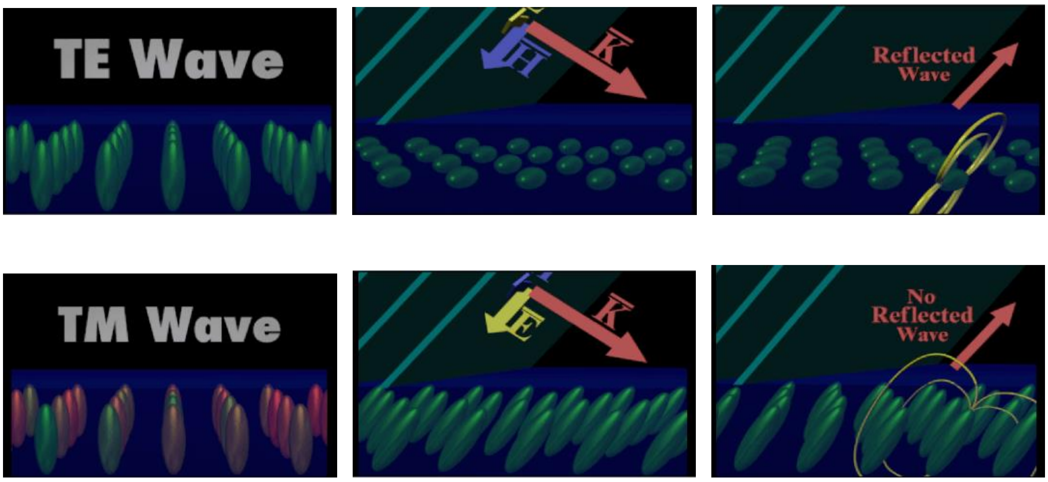

Figure 2.3. Wave fronts of E field normal to the plane incidence (TE Mode). Below, it shows the H field normal to the plane of incidence (TM Mode). (Figure is adapted from an animation on the web page of *www.ee.byu.edu/ee/em/brewster.htm.avi)*

Fig. 2.3 represents the reflection of E, H and k vectors for TE and TM modes. It states that there is no reflected power at a point on TM Mode. Brewster Angle just exists in TM Mode where there is no reflected power as illustrated in Fig. 2.3. This occurs because of the dipoles that create the reflected wave. When a TM wave hits an interface dipoles are induced in the material in the direction of the E field. At just the right angle the dipole axes line up with the direction of the reflected wave. Since a dipole does not radiate along it's axis, then no reflected wave generated. This happens when the reflected wave and the transmitted wave are perpendicular to each other.

For a perfect dielectric media, conductivity is assumed to be zero and the permeabilty is 1. From the Snell's law of refraction

$$\frac{\sin Qi}{\sin Qt} = \frac{k2}{k1} = \left(\frac{\varepsilon r2}{\varepsilon r1}\right)^{1/2} = n_{12} \qquad (2.32)$$

where n_{12} is the relative index of refraction. If $\varepsilon_2 > \varepsilon_1$, all the energy is transmit to the second medium. On the other hand if $\varepsilon_2 < \varepsilon_1$, $n_{12} \sin Qt > 1$, total reflection occurs on greater angles.

It is possible to simplify the Eq. (2.31) by using the Snell's law in Eq. (2.32) for perfect dielectrics

$$r_{||} = \frac{\tan(Qi - Qt)}{\tan(Qi + Qt)} \tag{2.33}$$

For the case (Qi+Qt) goes to π/2, then tan (Qi+Qt) goes to infinity and $r_{||}$ becomes 0. So the reflected and refracted waves are then normal to one another. Thus,

$$\sin Qt = \sin(\pi/2 - Qi) = \cos Qi \tag{2.34}$$

So the Eq. (2.32) becomes

$$\tan Qi = \left(\frac{\varepsilon r2}{\varepsilon r1}\right)^{1/2} = n_{12} \tag{2.35}$$

Eq. (2.35) defines the Brewster Angle.

Brewster angle can be detected in radar sections from the amplitude and phase variations. If the amplitude variations can be detected with the phase changes in radar data, relative dielectric constant of the deeper layer at that interface can be determined. The angle under which the amplitude decreases very strongly, determines the Brewster angle. Brewster Angle only arises in CMP sections in a non-conductive media. The break-down weakens itself with increasing conductivity. Decrease of amplitude is also accompanied by phase change of 180 degrees with only small or not conducting medium. In a non-conductive media a rapid phase change can be seen. In a more conductive media phase change can be seen on a large angle range. For this estimation relative permeabilty of the medium is accepted as 1 and the conductivity is accepted as zero. That means the media is assumed to be perfect dielectric.

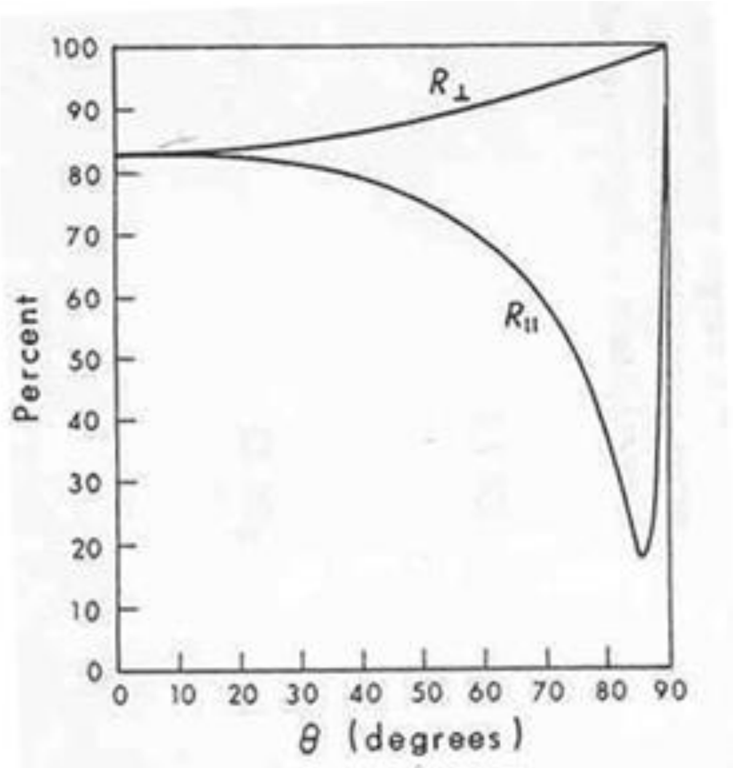

Figure 2.4. The power reflection coefficients R ⊥ and R || versus angle of incidence for plane waves at an air-sea interface. [2]

The magnitude and phase of reflection are rather different in TE and TM Mode. When the angle of incidence goes to 90 degrees the magnitude of both goes to 100 percent as illustrated in Fig. 2.4. Reflection coefficient for TE mode increases with increasing angle of incidence, whereas in TM mode the power of reflection coefficient falls abruptly to a minimum and increases again with the increasing angle of incidence.

For further information on the derivation of these equations electromagnetic theory books can be referred such as Stratton and Ward et al. [1,2]

2.3. Radiation Pattern Of A GPR Antenna

The used GPR system consists of an external PC, a recording control unit, a transmitter and a receiver antenna as shown in Fig.2.5. In ground penetrating radar, radiation is electromagnetic and its propagation is described by Maxwell's equations. When EM waves radiated from an antenna they may become polarized. The antenna determines the type of the polarization. Polarization of the antenna is taken to be the polarization in the direction of maximum gain. [8]

Figure 2.5. Components of a GPR system. Unshielded, bistatic, dipole antenna with its control unit and recording notebook computer.

The radiation pattern of an antenna is generally its most basic requirement since it determines the spatial distribution of the radiated energy [9]. Most of the GPR systems use a dipole antenna, which has strong directivity. These dipole antennas linearly polarize. In this discussion electric component, E is orthogonal to magnetic component H. Both of them are also orthogonal to the propagation direction. The specific shape and size of the directivity pattern lobes are functions of the dielectric constants of the present media. [5] The directivity patterns for a horizontal electric dipole show a three-lobed structure with sharp nulls in the E-plane (vertical plane containing the antenna element) and a scalloped two-lobe structure in the H-plane (vertical plane perpendicular to the antenna element) [10]. GPR antenna in a homogeneous and isotropic media radiates symmetrical electromagnetic field. An antenna on the surface of a homogeneous half-space, for instance on the air earth interface, GPR produces a highly directional radiation pattern. Waves transmitted with a GPR dipole antenna have a highly directional radiation pattern. It has a strong energy peak in direction of the critical angle of the air – earth interface. Radiation patterns are also different in perpendicular and parallel polarizations. Radiation pattern of a dipole in a homogeneous, and isotropic medium is represented in Fig. 2.6 [11]. Antenna in this system is located at the origin point of a coordinate system and extending along the x-axis. Figure at the left represents the perpendicular antenna orientation to the profile direction. And the other one represents the parallel antenna orientation. In parallel antenna orientation radiation of electromagnetic waves has three lobes. Energy of the antenna decreases in two points. But in perpendicular orientation energy decreases slowly without sharp energy losses.

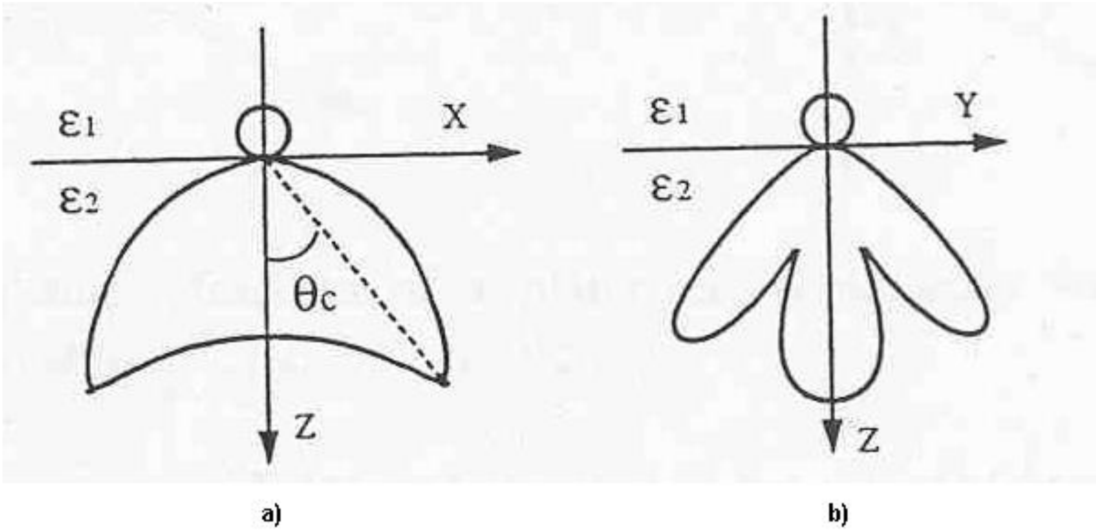

Figure 2.6. Radiation pattern of a dipole antenna. a) Perpendicular antenna orientation b) Parallel antenna orientation [11]

3. SITE CHARACTERISTICS

This thesis contains a part of Interurban Project of Berlin Technical University, which clarifies the dynamics of water and materials at urban locations. In order to map the water distribution as an aim of this project in the selected field, Ground Penetrating Radar measurements have been performed with a number of other geophysical methods such as geoelectrics, Spectral Induced Polarization (SIP) and Surface Nuclear Magnetic Resonance (SNMR) [12]. For this aim of this project, Tiergarten was selected which is typical for urban soils. Tiergarten is a metropolitan park with intensive use of pedestrians, sportsmen and big events such as 'Love Parade'. It is one of the biggest parks of the city, which is located in the middle of the Berlin. (Fig.3.1.)

The survey area covers a profile of 400 m. length starting at one of the most frequented roads in Berlin and goes deep into the park. End point of the profile is quite close to the small lake, which exists in the middle of this metropolitan park. Ground penetrating radar measurements contain a 90 m long part of this profile, from the points of 150m up to 240 m on this survey line. Fig 3.2 represents the map of the Tiergarten area. Red line on this map indicates the survey line at this area.

Figure 3.1. The diagram represents the Tiergarten in the middle of the city.

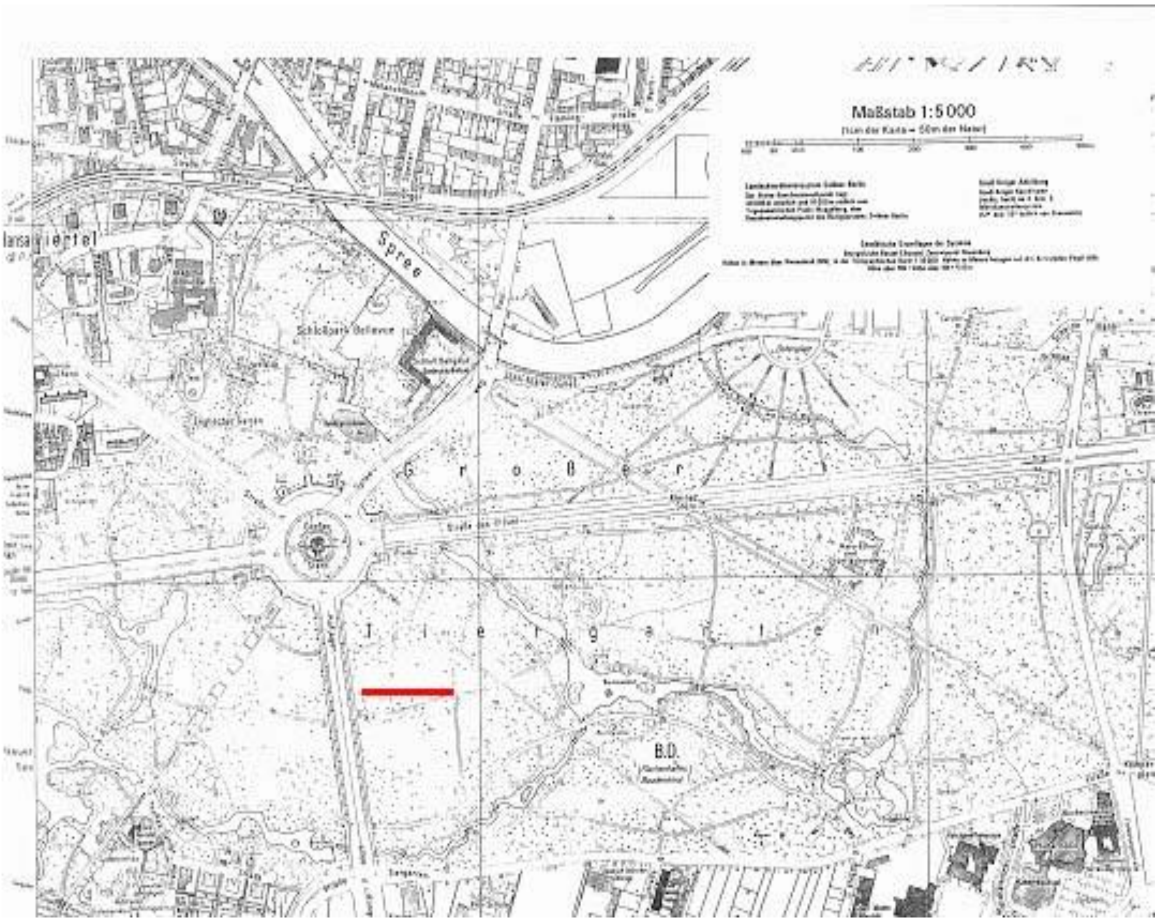

Figure 3.2. The map of the Tiergarten area.

The morphology of the park is quite regular and surface shows very smooth landscape at this region, as usual of the whole Germany. There is not any noise that can effect the measurements such as electricity, metro etc. The park is far from the settlement and it is full of huge, old trees.

Due to 3 major ice advances during the last 650000 years, the geology of this area, consists nearly solely of quaternary sediments. Today's structure and morphology is predominated by the latest glacial from 16-20000 years ago. The region to the west and north of Berlin is subdivided into tabular plates and partially water filled low grounds. Valley sands and gravels form the principal sedimentary structure for those filled morphologic depressions.

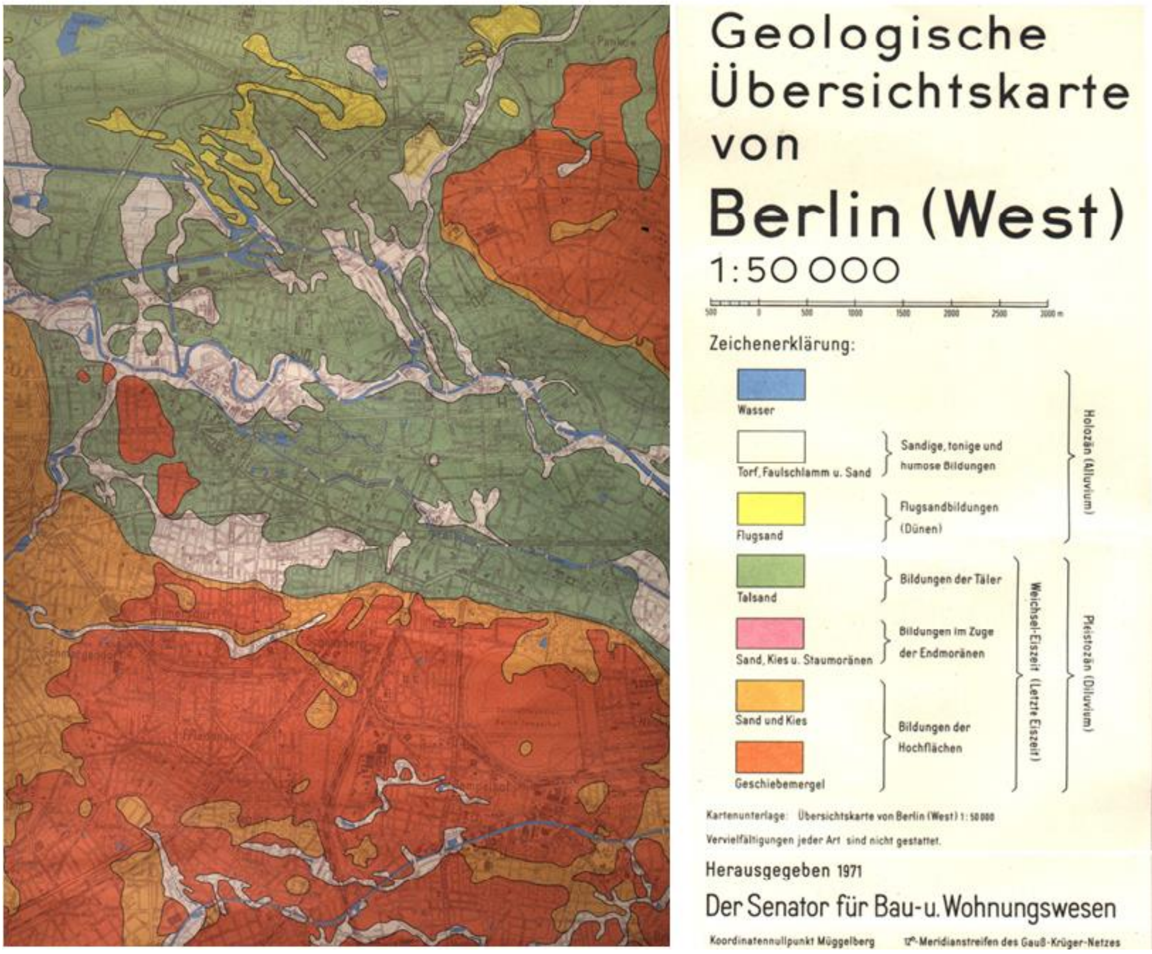

Figure 3.3. Geological map of West Berlin [13]

Fig. 3.3 represents the geological map of the West Berlin. Tiergarten locates in the middle of this geologic map. Figure represents that, the West Berlin consists of quaternary sands.

There are several bore-hole measurements which have been done at the vicinity of the test field after the 2nd World War [13]. The results of these measurements are quite similar within each other. Bore-hole measurement results state that the test area primarily composed of sand. In some regions, the upper parts of the field are filled with waste deposits, especially after the 2nd World War.

To investigate the field better, an area in the middle of the whole profile has been excavated. The dimensions of this excavated area was approximately one meter in width and 10 m in length. Up to 40 cm, test field is composed of humus. Under this shallow layer, the following material consists of sand as shown in Fig. 3.4. In the vicinity of two meter in depth, it is possible to detect the ground water intrusion at the field. There is a distinct passage to the ground water after the following depths.

Figure 3.4. Excavated area in the test field.

4. FIELD MEASUREMENTS

4.1. Constant Offset Measurements

4.1.1. Methodology

GPR measurements were performed with RAMAC GPR device of MALA GEOSCIENCES. 50, 100, 200, 400 MHz antenna frequencies with bistatic, unshielded antennas selected to compare the differences on radargrams with respect to frequency changes. Normally, reflection profiling mode is used in the radar measurements. Profiling by GPR is similar to sonar and seismic reflection surveying. Different modes such as common midpoint (CMP), wide-angle reflection and refraction (WARR) and transillumination can be also used in radar surveys. These modes can be used to determine the signal velocity and attenuation in the ground [6]. During this work, reflection profiling and CMP measurements were performed with different antenna frequencies and with a variety of antenna orientation.

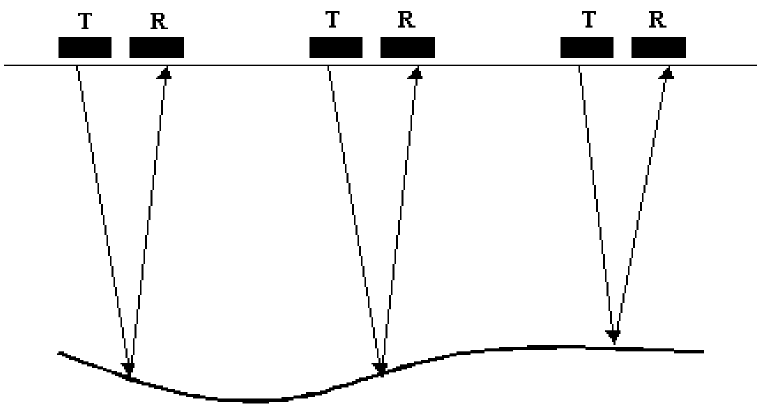

Figure 4.1. Constant offset measurements.

In principle ground-penetrating radar is similar with reflection seismic technique, except that it is based on propagation and reflection of transient EM energy. Short pulse of electromagnetic energy is transmitted into the ground. Propagation of radar signal primarily depends on the high frequency electrical properties of the ground. Change of electrical properties in the ground cause the transmitted signal to be reflected. If the time for the pulse to go to the reflector in the ground and return to the receiving antenna (two way travel time) is measured, the position of the reflector can be determined. For this, the velocity of the pulse must be known [14]. Fig. 4.1 illustrates the constant offset measurements in radar with a fixed offset between antennas. Two antennas moved along a profile with this fixed antenna separation.

A variety of antenna orientation performed during the measurements as shown in Fig. 4.2. Perpendicular broadside, parallel end fire, parallel broadside and cross polarization 1 and 2 are the antenna orientations that were used in constant offset measurements. Perpendicular broadside is the most common antenna orientation in which two antennas are parallel to each other and both of these antennas are perpendicular to the profile direction. The other antenna orientations were also used to compare the results with respect to different polarization.

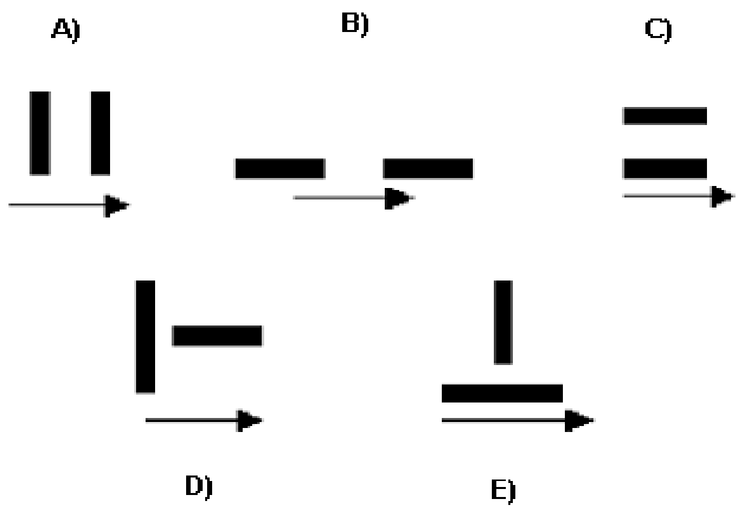

Figure 4.2. Antenna orientations which were used in field measurements. a) Perpendicular broadside, b) Parallel end fire, c) Parallel broadside, d) Cross-polarization 1, e) Cross -polarization 2.

Constant offset (reflection profiling) measurements were performed in two parts. One of the measured profiles was from 150 m up to 180 m. The other part was measured from 187 m. up to 240 m because of a thin road in the middle of the profile it wasn't possible to complete the measurements in one section. Each antenna orientation was used with a variety of frequencies to compare the results. Transmitter - receiver (antenna) offset is one of the main parameters to determine when designing a GPR survey. Recorded amplitudes ultimately decrease with offset through dominance of the geometrical spreading and attenuation terms. Thus, there is a recording offset that maximizes the reflected amplitude, and this offset will be different for each reflector. Antenna offset was determined according to the chosen antenna frequency and according to the behavior of the reflector [15]. Time window is one of the other parameter that must be determined by the user before the measurements. In these measurements time window did not keep same for all measurements. It has been changed in each of the frequency because of the limited penetration depth up to higher frequencies.

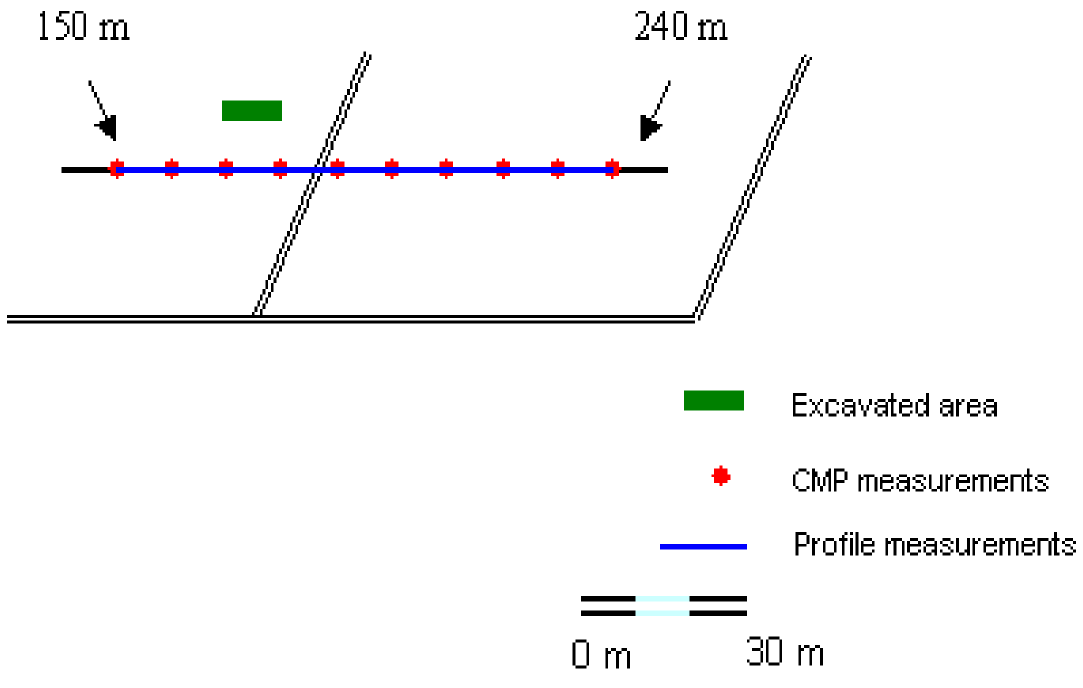

Figure. 4.3. Illustration shows the schematic diagram of survey area.

Fig. 4.3 represents a schematic diagram of the test site with the survey line and measured profiles on it. Red points indicate the each CMP location with 10 meters between each of them. Green rectangle box indicates the excavated area in the test field. Blue lines represent the survey lines for the reflection profiling measurements in between 150 – 180 m and 187 - 240 meter. GPR measurements were performed from the point of 150 meter up to 240th meter in the Tiergarten area, as presented in Fig. 4.3. This public park has an intensive use by pedestrians. The survey area covers a profile of 90 m length from the side of main road and goes deep into the park. Fig. 4.4 presents the field application of constant offset measurement along the profile with 200 MHz frequency antennas in parallel broadside orientation. In parallel broadside orientation transmitter and receiver antennas are parallel to each other and they are both parallel to the profile direction as shown in Fig.4.4. The yellow steel tape measure, on the surface indicates the survey line at the field.

Figure. 4.4. Field application of constant offset measurement along the profile with 200 MHz frequency antenna in parallel broadside orientation.

4.1.2. Data Processing

Processing of the data have done with the program REFLEX of the version 2.5. This software can be used not only for radar data interpretation but also in forward modelling and tomograpy of radar data and also interpretation of seismic data.

When data is succesfuly recorded at the field, the first step in procesing is data editing. In the first step the raw data, which is present in a RAMAC format, imported into REFLEX format. After that, data editing can be done. Data editing encompasses issues such as data reorganization, data file merging, data header or background information updates, repositioning and inclusion of elevation information with the data. Extensive explanation of GPR data processing has been done by Annan [16].

Basic processing steps take place after data editing processes. The initial basic processing step is usually temporal filtering, which is referred as ‘dewow’, to eliminate very low frequency components from the data. These kind of frequencies are associated with either inductive phenomena or possible instrumentation dynamic range limitations. Declipping process is used to edit the declipped data. Clipping is done according to the amplitude values of each trace. Ater this, suitable gain is selected and applied to the data. Amplitude loss of EM waves due to the absorption and spherical divergence can be balanced by gain processing. And the low frequency noise must be eliminated with a band pass filter. When bandpass filter applied to the data before gain, ghost signals at the beginning and end of each signal can be generated. If the gain applied to data before the filter there may be losses in some important signals. So the data processing steps must be selected carefully.

It is most of the time, operator’s choise to aplly advanced data processing. These processes include well known seismic processing operations such as trace attribute analysis, FK filtering, normal move out correction, deconvolution, migration and velocity semblance analysis which are discussed in a great deal of detail in Seismic processing series of Yilmaz [17].

A time migration of a two-dimensional profile on the basis of a constant velocity is performed in migration adaption to the data. The profile must represent a so called zero-offset profile, i.e. shot and receiver have to be at the same location. The goal of the migration is to trace back the reflection and diffraction energy to their original locations.

The fk filter can be used - though computing time intensive - as lowpass, highpass, bandpass or notch filter. It is highly effective for the suppression of noise with a certain dip in the data set. Like this, horizontal noise signals, as caused for example by reverberations, can be suppressed by cutting the wavenumber zero from the filter area. In an analog way correlated signals with desired gradients can be emphasized.

4.1.3. Results

In this section, constant offset field applications and individual results of these field measurements take place. More detailed discussion with the comparison of other parts will take place at the end of the thesis.

On the survey line from 187 m up to 240 m a set of radar measurements have been carried out with different antenna orientation and frequency. Antenna offset was fixed as 1 m for 100MHz, 200 MHz and 400 MHz frequencies. Fig. 4.5, 4.6 and 4.7 illustrate the perpendicular broadside antenna orientations with 100, 200 and 400 MHz frequencies, respectively. This is the most common antenna orientation used in radar surveys. x - axis represents the distance in meter, y-axis represents the depth scale in ns in each radargram. First arrival of the waves at the top of the radargram, which exists as a black direct line, is the air wave. Ground wave exists under the air wave, which is recorded as the second arrivals, propagating in the subsurface along the earth surface. There are some significant facts about the characteristics of the ground wave. The ground wave has the opposite phase to the air wave. The ground wave amplitude decays faster with distance than the reflected waves. Due to conductive loss in the earth, ground wave diminish with increasing subsurface conductivity. Ground wave in GPR has a wide variety of applications in determination of water content (e.g. Shuchun Du) [11]. Black horizontal lines in the vicinity of 40 ns are the reflections from the ground water, which exists in approximately two meters. When the velocity of this media, which is accepted as 0.1 m/ns for ordinary soil, is adapted to this radargram it corresponds to a depth of 2 meters. This states that the water table depth determined from radar section is in quite coincidence with field samples and borehole measurements.

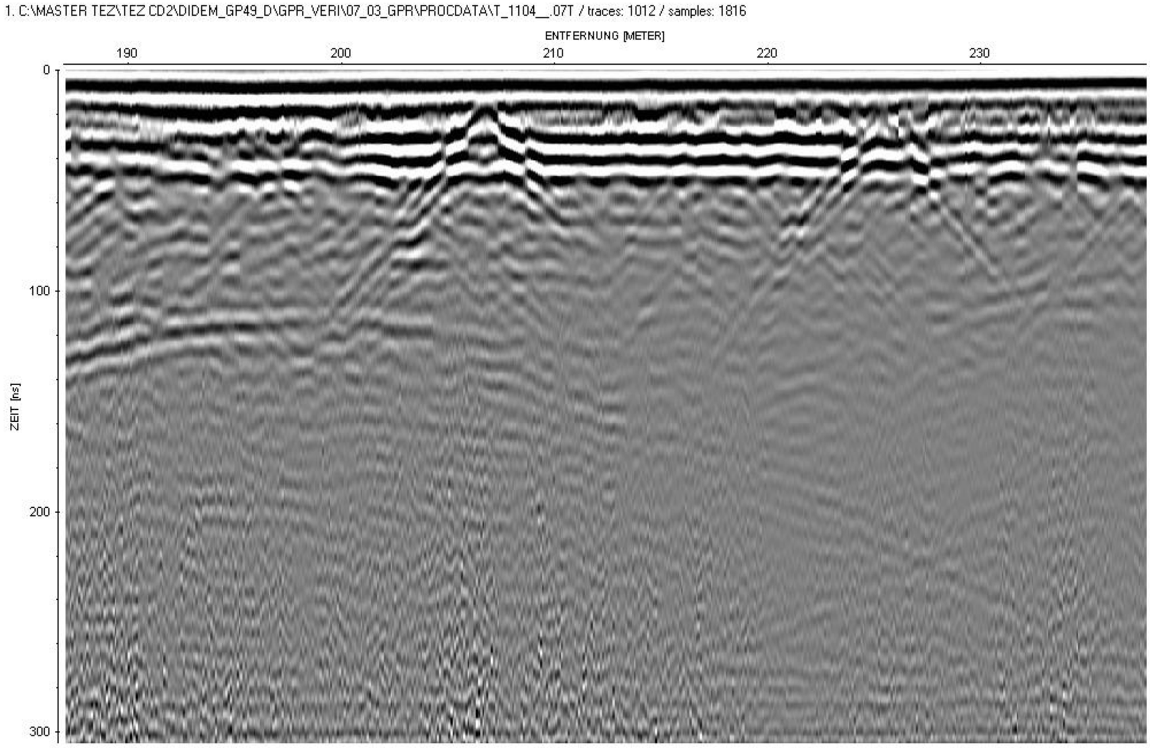

Fig. 4.5. Perpendicular broadside antenna orientation with 100 MHz antenna frequency.

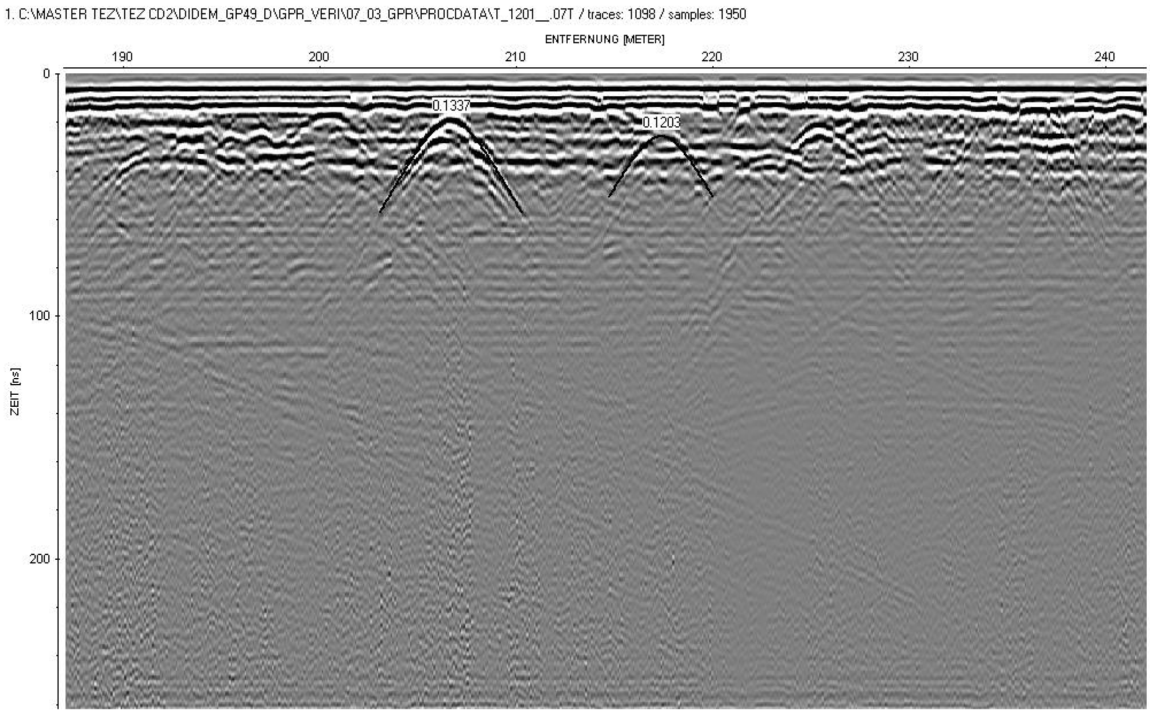

Fig. 4.6. Perpendicular broadside antenna orientation with 200 MHz antenna frequency.

A number of hyperboles can be seen on the radargrams in Fig. 4.5, 4.6 and 4.7. These hyperboles indicate the reflection from buried objects such as metallic pipes. In this test site, these reflections are caused by the thin water pipes in a shallow depth of up to 1 m. These diffraction hyperboles can be seen in clearly with these each three frequencies. Velocity analysis can be done to these diffraction hyperboles as in Fig. 4.6. This can be done with the hyperbole adaptation procedure of the software REFLEX. With the help of this velocity analysis procedure best hyperbole can be intersected to the diffraction hyperboles on the radargram. Propagation velocity information for this media can be determined by this way. In Fig. 4.6 the velocities of 1.2 m/ns and 1.3 m/ns on the diffraction hyperboles represent the velocity of the subsurface material at that point. By the change in velocity of that material, the shape of these hyperboles also varies.

Each radargram in Fig 4.5, 4.6 and 4.7 gives different depth information with respect to each other. It is known that the penetration depth increases with the decrease of frequency. However, resolution increases with increasing frequency. By using low frequencies in radar surveys high penetration depths can be obtained, but the resolution will be poor. Using very low frequencies to obtain a high penetration depth can cause to miss small targets in the field. Thus the operator must be careful in frequency selection. Optimum frequency must be selected according to the aim of the work. In these examples time window is different in each of the radargram. So, the penetration depth and resolution is not same for all measurements. In Fig. 4.5 with 100 MHz antenna frequency, time window has been selected as 300 ns. As the frequency increases the depth of penetration will decrease. So, in Fig. 4.6 with 200 MHz antenna frequency the time window increased to 260 ns. And finally in the measurement with 400 MHz frequency the time window was selected as 130 ns. These different time windows correspond to different depths in penetration. This means that in Fig. 4.5, Fig. 4.6, and Fig. 4.7 the end point in depth does not corresponds to the same depth scale. These situations must be taken into consider when comparing the different frequency applications of same orientations.

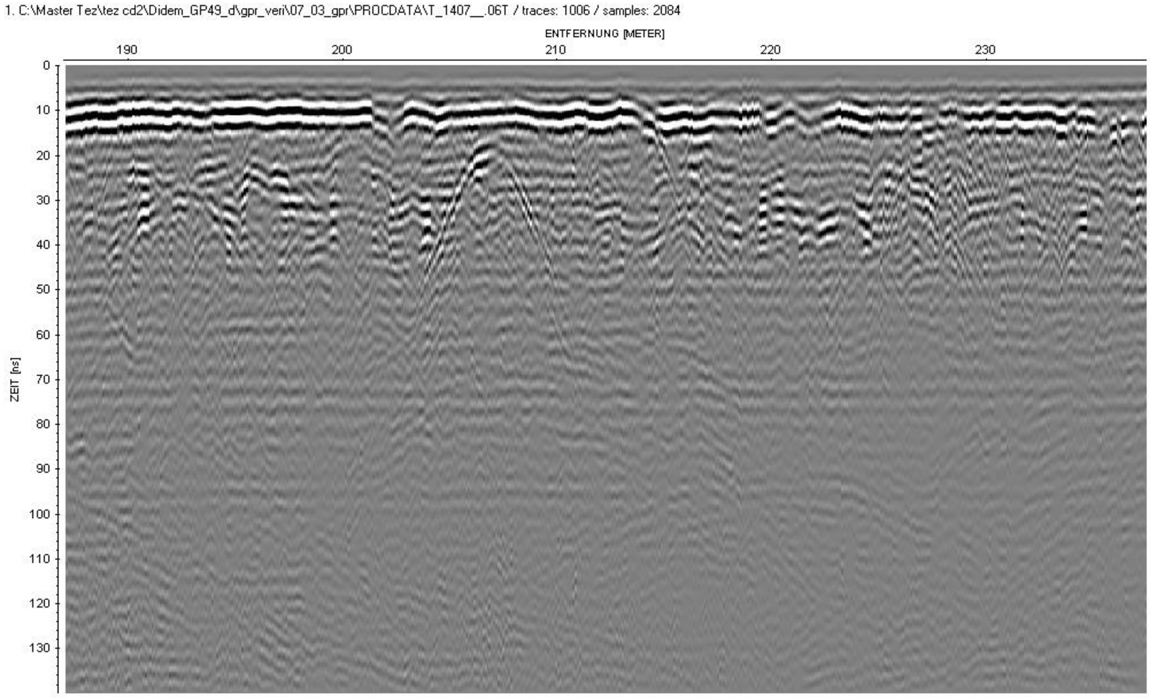

Fig. 4.7. Perpendicular broadside antenna orientation with 400 MHz antenna frequency.

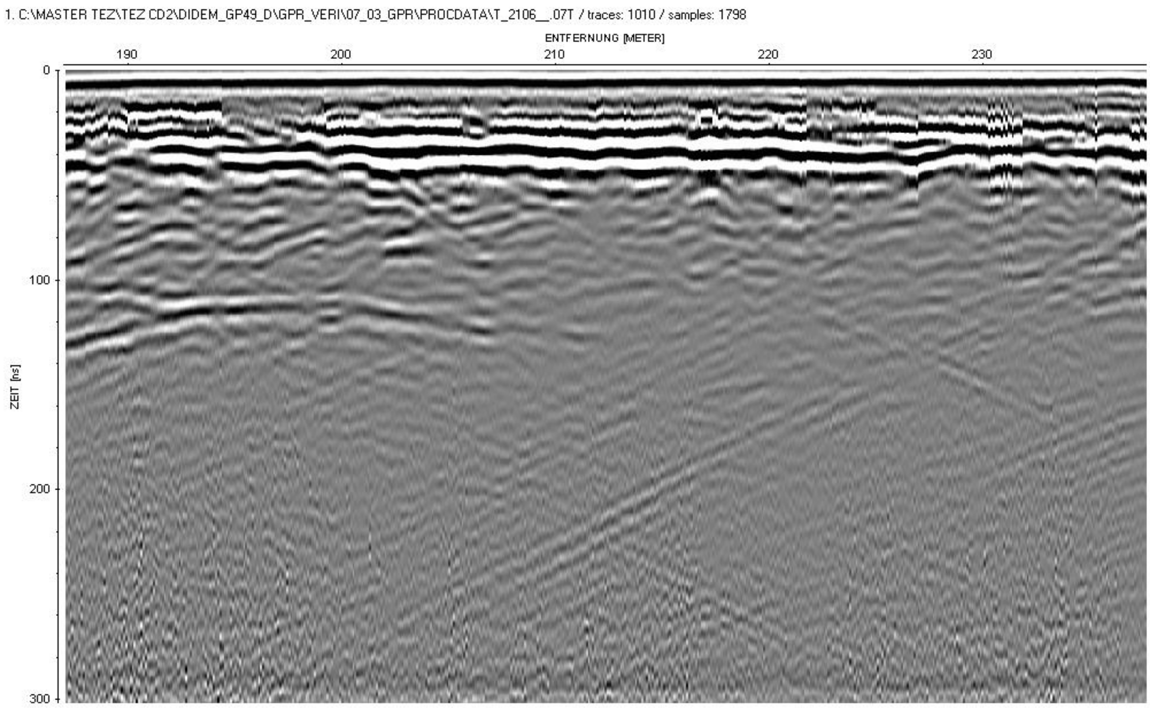

Fig. 4.8. Parallel broadside antenna orientation with 100 MHz antenna frequency.

Fig. 4.8, 4.9 and 4.10 illustrate the parallel broadside antenna orientations. 100, 200 and 400 MHz frequencies have been represented in these figures, respectively. These three radargrams have different frequencies so the penetration depth is also different in all of them. Time window has been selected different in each of the measurements according to the frequency selection. In Fig.4.8 with 100 MHz frequency antennas, selected time window is 300 ns. This radargram gives information up to a depth of approximately 200 ns. This corresponds to a depth of 5 meters when constant velocity of 0.1 m/ns assumed. The reflection beneath the 100 ns can be detected easily in Fig. 4.8. In Fig. 4.9 with 200 MHz antenna frequency the time window is nearly 260 ns. But there is just background noise and multiple reflections after a depth of 120 - 140 ns. The reflections from water table are rough and not continuous in this radar section. There are ghost signals at the bottom of the radargram, which is caused by the processing procedure. The reflection on Fig. 4.8 cannot be seen with this antenna frequency because of the penetration depth limitation.

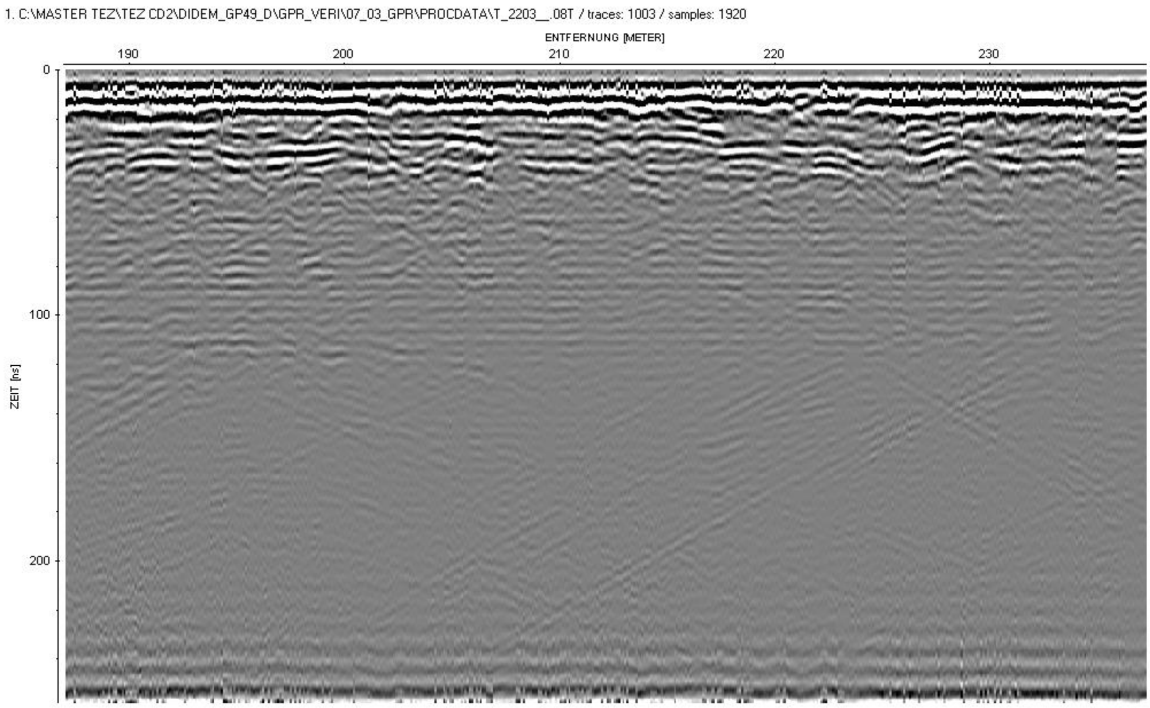

Fig. 4.9. Parallel broadside antenna orientation with 200 MHz antenna frequency.

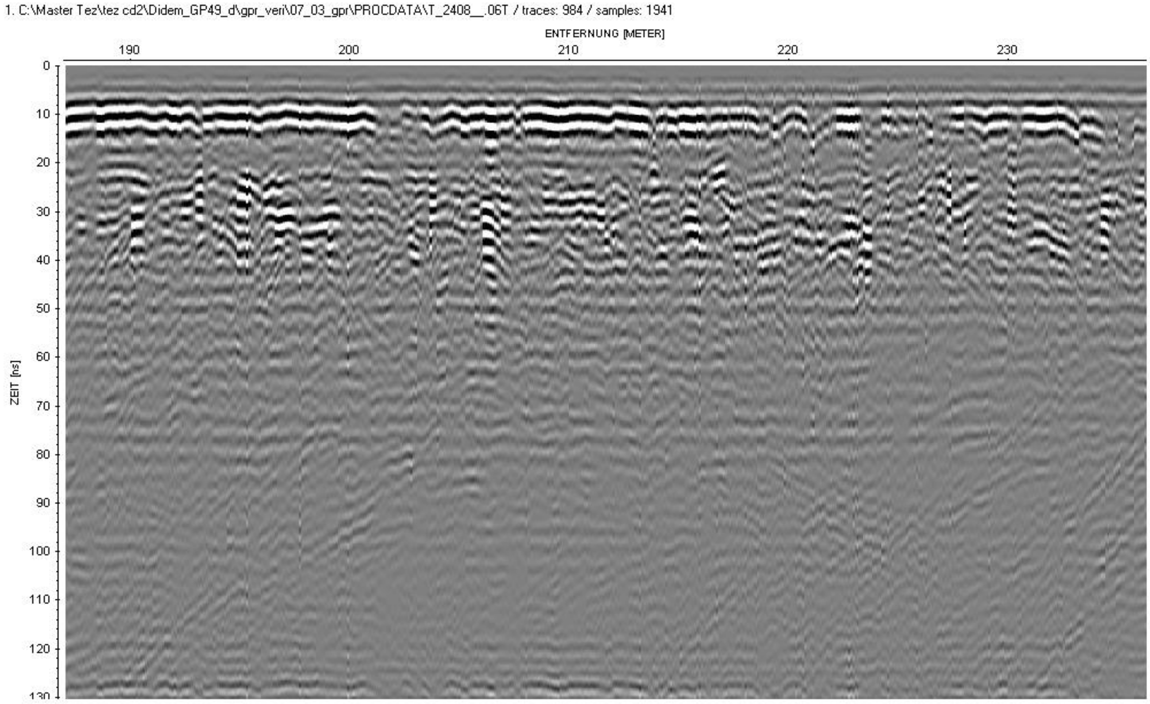

Fig. 4.10. Parallel broadside antenna orientation with 400 MHz antenna frequency.

Fig 4.10 represents the parallel broadside antenna orientation with 400 MHz antenna frequency. This antenna frequency gives a very limited depth of penetration. But the subsurface can be seen with a better resolution. In Fig. 4.10 time window is just 130 ns and this corresponds to a depth 5 or 6 meters approximately. Water reflections in the vicinity of 40 ns can be clearly identified. Ground wave at the top is also powerful. But the information below the 100 ns is insufficient. Strong reflection in Fig 4.8 at 120 ns cannot be seen in this measurement. By using 200 MHz frequency it can be very difficult to detect at 120 ns. After this depth there is no real information from the subsurface in Fig. 4.9. In figure with 400 MHz frequency this strong reflection is at the end of the time window. Existence of the diffraction hyperboles in each frequency of the perpendicular antenna orientation must be caused by the different polarization with this orientation compared to the parallel antenna orientation. The non-existence of the diffraction hyperboles in Fig. 4.8, 4.9, and 4.10 can just be due to the change in antenna orientation.

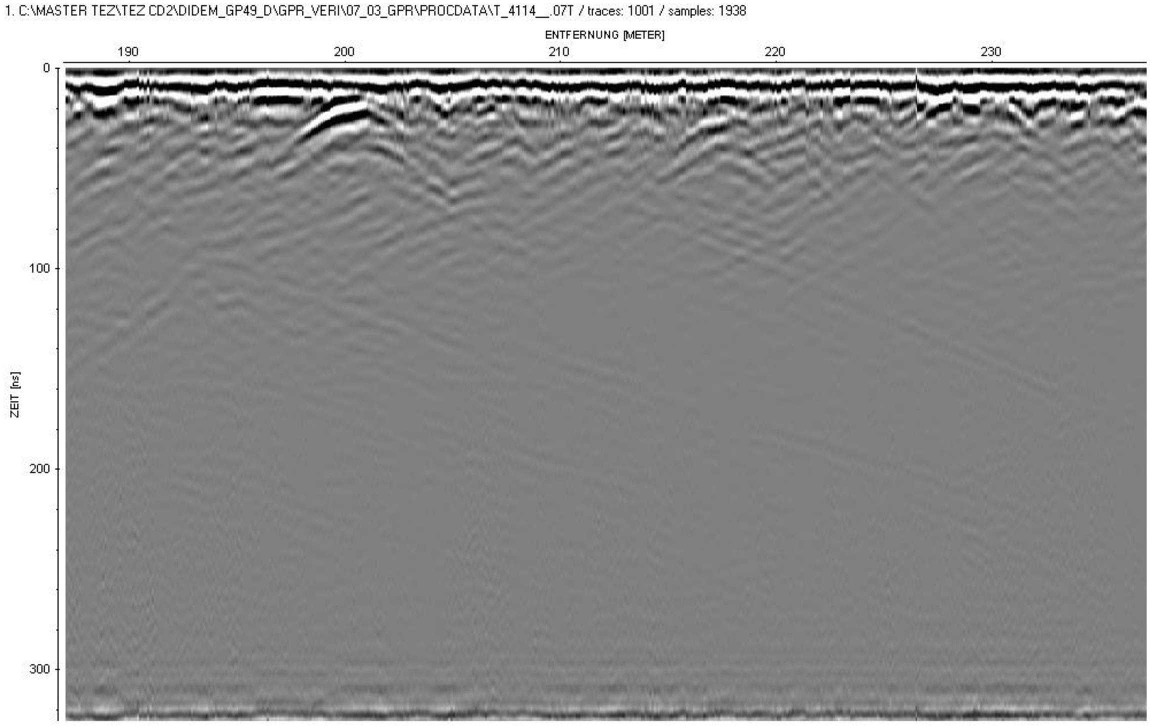

Fig. 4.11. 100 MHz antenna frequency by using cross-polarization 1, antenna orientation.

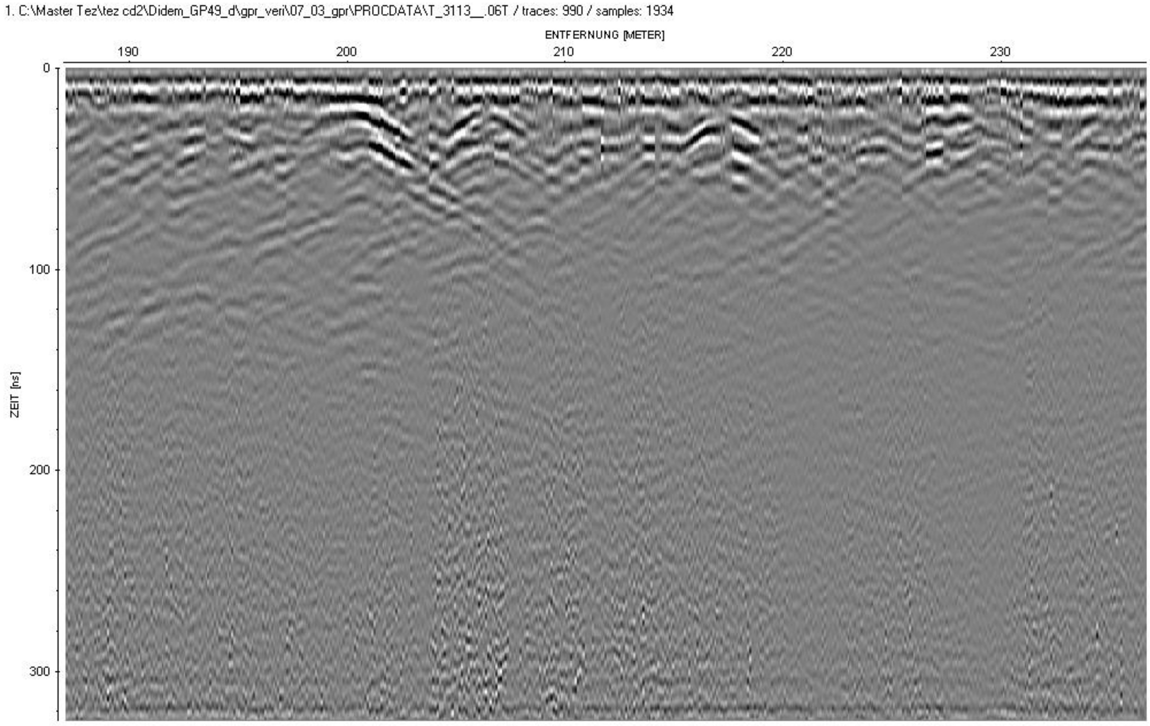

Fig. 4.12. 100 MHz antenna frequency by using cross-polarization 2, antenna orientation.

Fig. 4.11 represents the cross polarization 1, antenna orientation measurement. This antenna orientation normally does not used in GPR measurements. In this measurement receiver antenna was parallel to the profile direction and it was perpendicular to the transmitter antenna as illustrated in Fig. 4.2. With analogous to this, Fig. 4.12 represents the cross polarization 2, antenna orientation measurement in which the transmitter antenna was parallel to the profile direction and it was perpendicular to the receiver antenna as illustrated in Fig. 4.2. Both of these figures represent 100 MHz frequency antenna measurements. In this study, it was a special interest to study different antenna orientations. In both of these measurements there are not so much information. Neither ground wave nor the air wave can be seen continuously. Reflections and diffraction hyperboles are rough and irregular. Even water reflections are undetectable with these two antenna orientations.

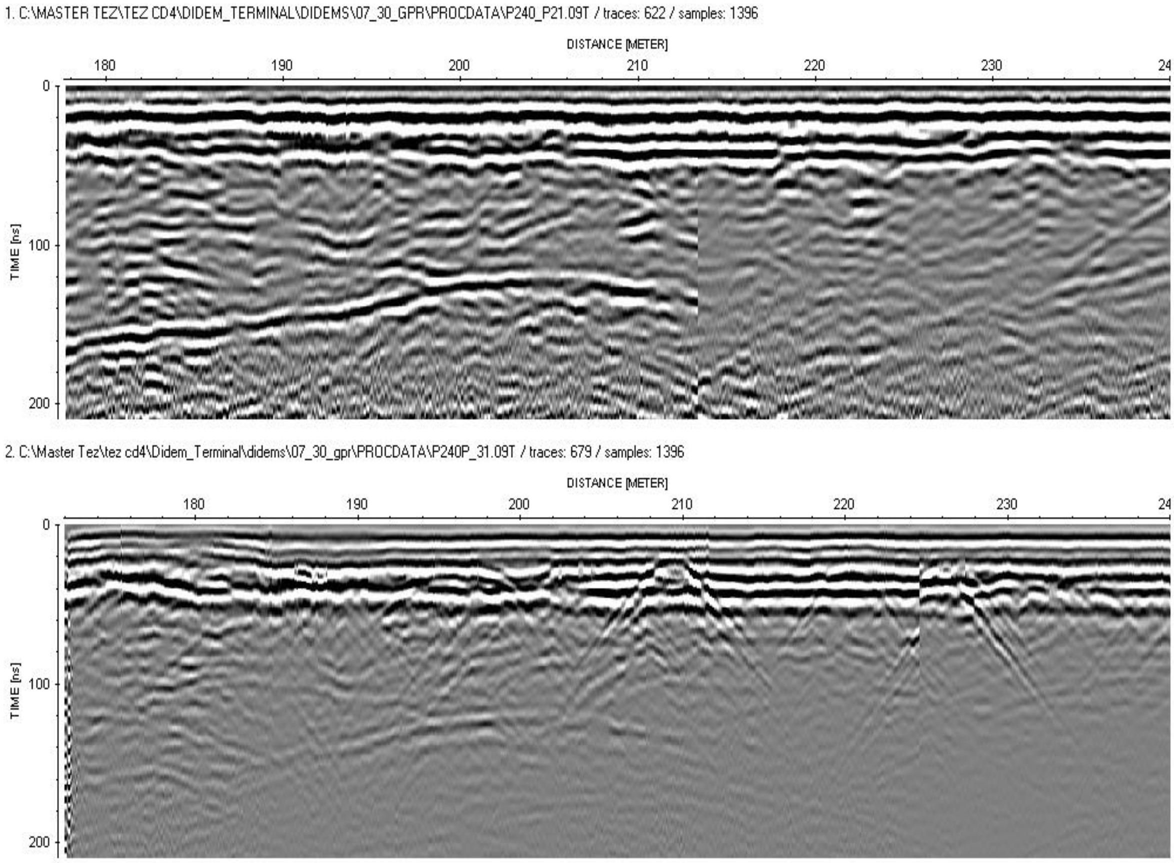

Figure 4.13. 100 MHz antenna frequency, by using parallel end fire antenna orientation (above) and perpendicular broadside antenna orientation (below).

Fig. 4.13 represents two radargrams from the test field, beginning in the 240th meter and goes up to ≅ 170 meters on the profile direction as represented in Fig. 4.3. Both of them are 100 MHz frequency antennas by using parallel end fire (above) and perpendicular broadside antenna orientations (below) at the test field. With parallel end fire antenna orientation, air wave, ground wave and reflections from the ground water intrusion can be detected clearly. There is another reflection detected with this antenna orientation beginning from 178 m up to 212 m along the survey line. This reflection has a depth of 120 to 140 ns. This is the strongest reflection in this radargram. This reflection is supposed to cause from the change in subsoil characteristics at this depth. Diffractions hyperboles cannot be detected with this antenna orientation as the measurements in Fig. 4.8, Fig. 4.9 and 4.10. But the amplitudes of the reflections are better with compared to perpendicular antenna orientation. By using perpendicular broadside antenna orientation water pipes at the shallow subsurface can be determined clearly as the measurements in Fig. 4.5, Fig. 4.6 and Fig. 4.7. The locations of the pipes are in good agreement with the other measurements. But the reflection detected in parallel end fire orientation, can be detected slightly.

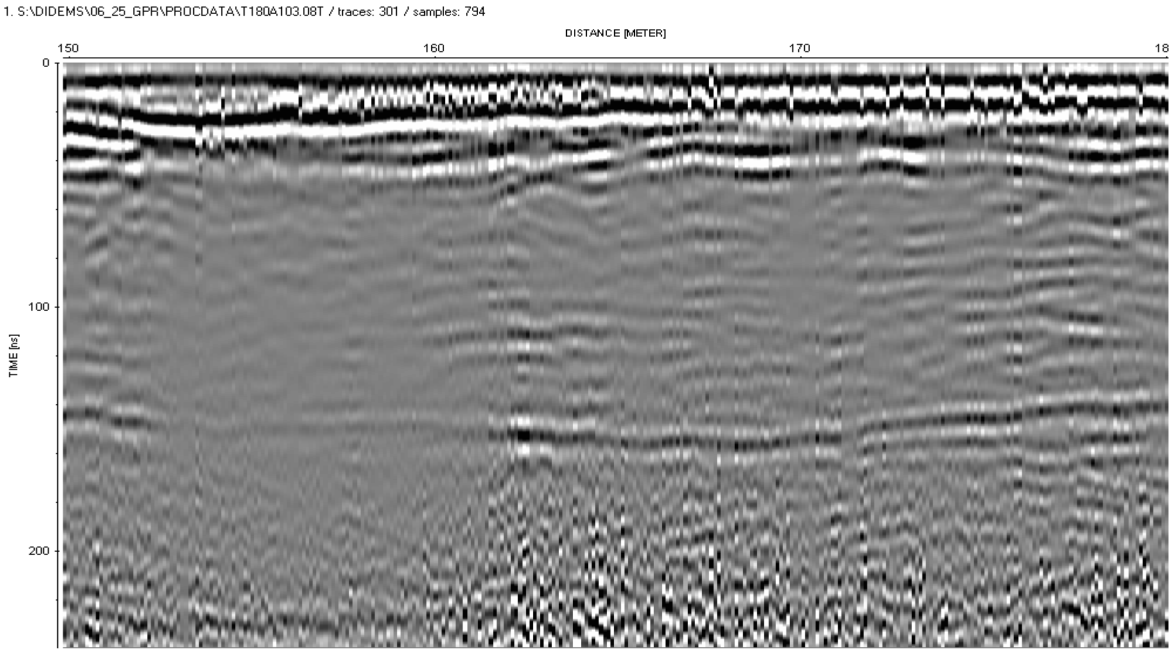

Figure. 4.14. 100 Mhz antenna frequency with parallel broadside antenna orientation on the profile from 150 m up to180 m.

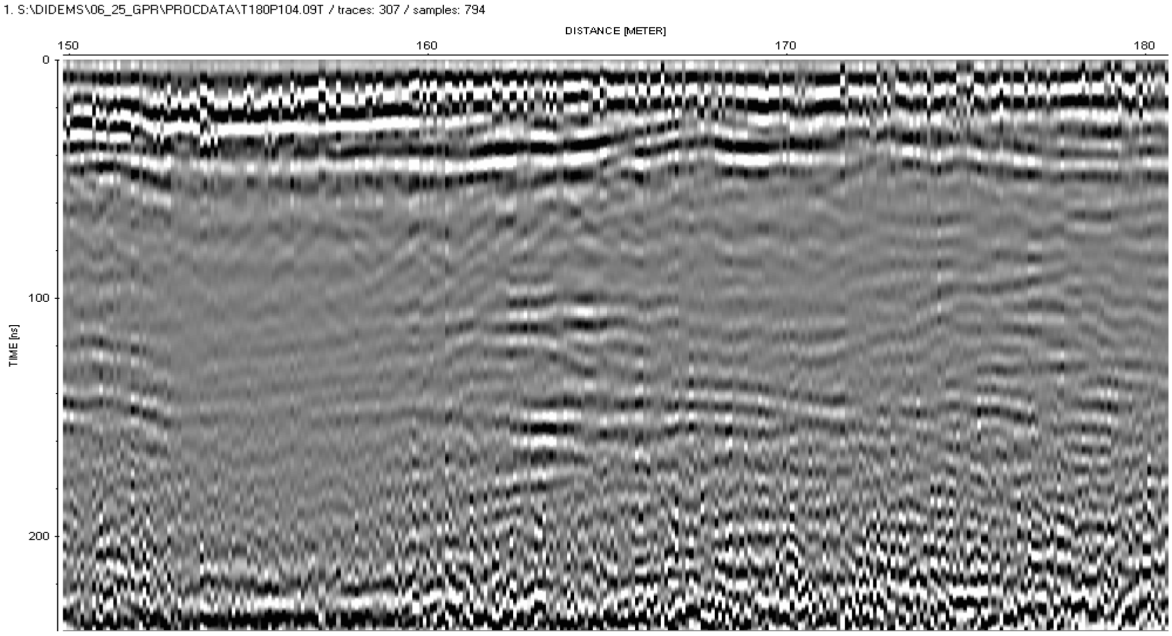

Figure 4.15. 100 MHz antenna frequency with perpendicular broadside antenna orientation on the profile from 150 m up to180 m.

Fig. 4.14 and 4.15 represents constant offset profile measurement at the field from 150 m up to 180 m as illustrated in Fig. 4.3. 100 MHz antenna frequency was selected with an antenna seperation of 1 m. Fig 4.14 represents the parallel broadside antenna orientation. Air wave takes place at the top of the radargram with a continuous direct line along the profile. Ground wave follows the water content and goes to deeper parts at the left side of the radargram as presented at the same figure. There is a strong reflection at the 140 ns that goes to deeper in the middle of the radargram. This reflection seems to be similar with the reflection in Fig. 4.13, and it continues along the profile. This reflection is supposed to be a dielectric contrast at the subsurface of the earth. This reflection gets weaker in between the points of 150 and 160 m. This weakness of the signal caused by the abundance of ground water at more shallower depth with respect to the right side of the radargram. Fig. 4.15 represents the perpendicular broadside antenna orientation. Reflections from ground water can be detected easily. In this measurement the reflection from the subsurface at 140 ns is more week and irregular with respect to parallel broadside antenna orientation. It can be hardly detected.

4.2. Variable Offset Measurements

4.2.1. Methodology

Common midpoint (CMP) and wide angle reflection and refraction (WARR) modes, which are the examples of variable offset measurements, are used in radar surveys to determine the signal velocity and attenuation in the ground. In this study CMP measurements have been performed to determine the velocity structure and also to detect the Brewster angle as presented in Fig. 4.16. CMP measurements have been carried out to determine the radar signal velocity versus depth in the ground with respect to antenna seperation at a fixed location. In the application of CMP measurements antenna seperation of two antennas changed according to a ‘common midpoint’ in the middle of the transmitting and receiving antennas. These surveys measure the change of two-way travel time from the reflections [6].

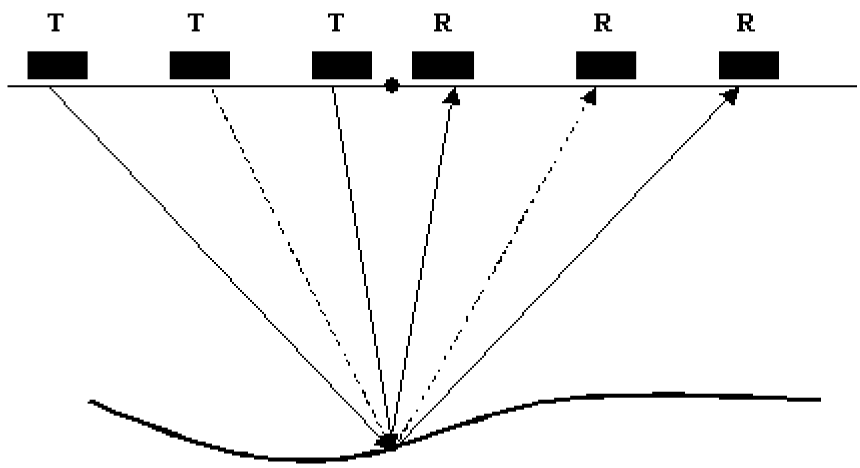

Figure 4.16. Common midpoint (CMP) measurements.

In this present work CMP measurements were performed with 50, 100, 200, 400 MHz frequency unshielded, bistatic antennas. Perpendicular broadside and parallel end fire antenna orientations, as illustrated in Fig. 4.2, were selected to perform the CMP field measurements. In most of the applications 0,2 m trace increment selected for the measurements. At ten different locations, as illustrated in Fig. 4.3, CMP measurements were performed with different antenna frequencies and different antenna orientations. To identify the Brewster angle and then to determine dielectric permittivity ratio of the interface, was the main aim of this study. Brewster angle can just be seen at parallel end fire antenna orientation, which is analogous to the transverse magnetic, TM mode. So, it was the main interest to focus on parallel end fire antenna orientation.

4.2.2. Data Processing

Processing of the CMP data have been done with the program REFLEX 2.5. Processing of the data have been done with 2-D data analysis procedure of the software. Then the velocity analysis have been applied to the data. In data processing, similar steps with constant offset data processing were used for variable offset data, as discussed in section 4.2. Data editing take the first place in preprocessing of CMP data. Any trace can be corrected individually if it is necessary. After that, suitable filter and gain processing applied to the data. In CMP data the clipped data takes place at the very first few traces so the declipping process doesn’t used in the processing of CMP data. It is important that the migration or deconvolution can’t be used for CMP data. At the end, velocity analysis of CMP data takes place. Velocity analysis has been done by the 1-D velocity analysis procedure of the software. The velocity analysis of the processed data from the test field takes place in the following chapter with its results.

4.2.3. Results

Variable offset field measurements, processing and velocity analysis of the CMP sections and individual results of these field measurements take place in this section. More detailed discussion, with the comparision of other parts, will take place at the end of the thesis.

In the field applications a variety of antenna frequencies have been used with parallel end fire and perpendicular broadside antenna orientations. CMP measurements in the field measurements used to utilize the velocity structure of the subsurface. In this study, it was the main aim to detect the Brewster angle with parallel end fire antenna orientations. So, two different antenna orientations have been performed to detect the Brewster angle and to investigate the difference within these antenna orientations.

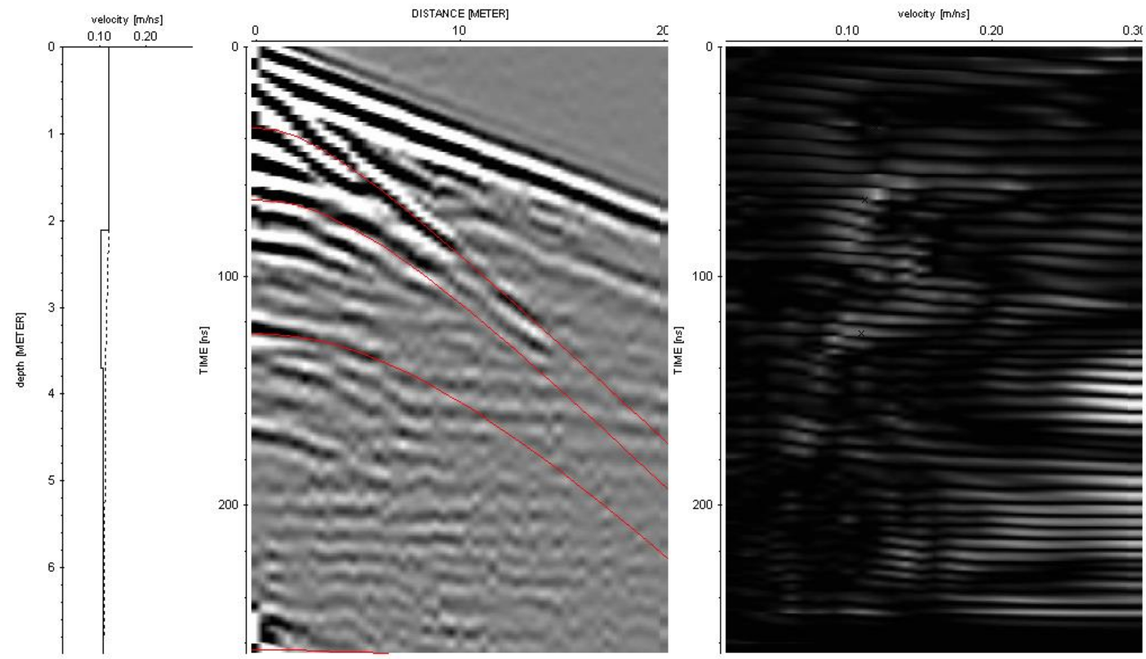

Figure 4.17. CMP measurement with 100 MHz frequency by using parallel end fire antenna orientation at the location 170 m.

On each 10 m, as illustrated in Fig 4.3, CMP measurements have been carried out with four different antenna frequencies and two different orientations. Measurements begin at a fixed point without any antenna distance between the transmitter and receiver. Then at each trace the transmitter and receiver distance have been increased up to a limited distance. The trace increment has been selected as 0.2 m for most of the measurements. Time window has been selected according to the used antenna frequency.

Fig. 4.17 represents the CMP measurement with 100 MHz frequency by using parallel end fire antenna orientation. The location of the measurement is at 170 m with a twenty meters of spacing and 0.2 m of trace increment. In the figure at the middle the radar section of the CMP measurement takes place. Velocity depth model for this section takes place at the left. This velocity depth model has been obtained by the velocity analysis of REFLEX by using the velocity semblance which is represented at the right. In the radar section, air wave has an evident linear shape at the top. Ground wave has a similar shape with a different velocity. The reflections from the dielectric constrats of the underground structure has a hyperbolic shape at the deepher parts.

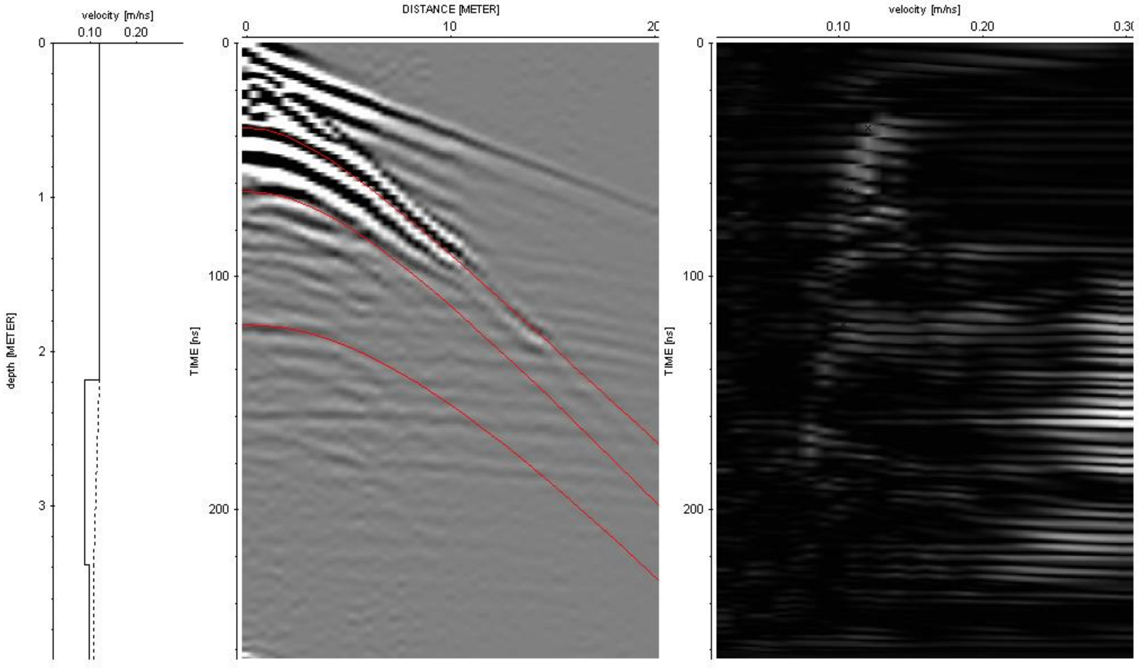

Figure 4.18. CMP measurement with 100 MHz frequency by using perpendicular broadside antenna orientation at the location 170 m.

Fig 4.18 represents the CMP measurement of the same location with the same antenna frequency. Every parameter has been selected the same of the preceiding measurement but the antenna orientation was the perpendicular broadside one. Air wave and the reflections from the ground water table can be detected clearly. Reflections from the ground water intrusion exists at the same depth scale, with the ground wave. So, there is an intersection of these waves at a depth of 40 ns on the CMP section. When we look at the velocity depth model of these measurements the velocity of the radar waves decreses after a depth of 2 meters because of the existence of ground water at this depth. The veloctiy of the radar waves decreses up to 0.7 m/ns by increses of dielectric permittivity of the saturated sand. There is another dielectric contrast under the ground water table, with higher velocity with respect to the ground water velocity. This velocity change dependent on the change in dielectric constant. It is already known that the change in dielectric permittivity cause the change in radar velocity. This increase of velocity at this depth can be caused by a physical change in material such pore size, porosity change or etc. at this location.

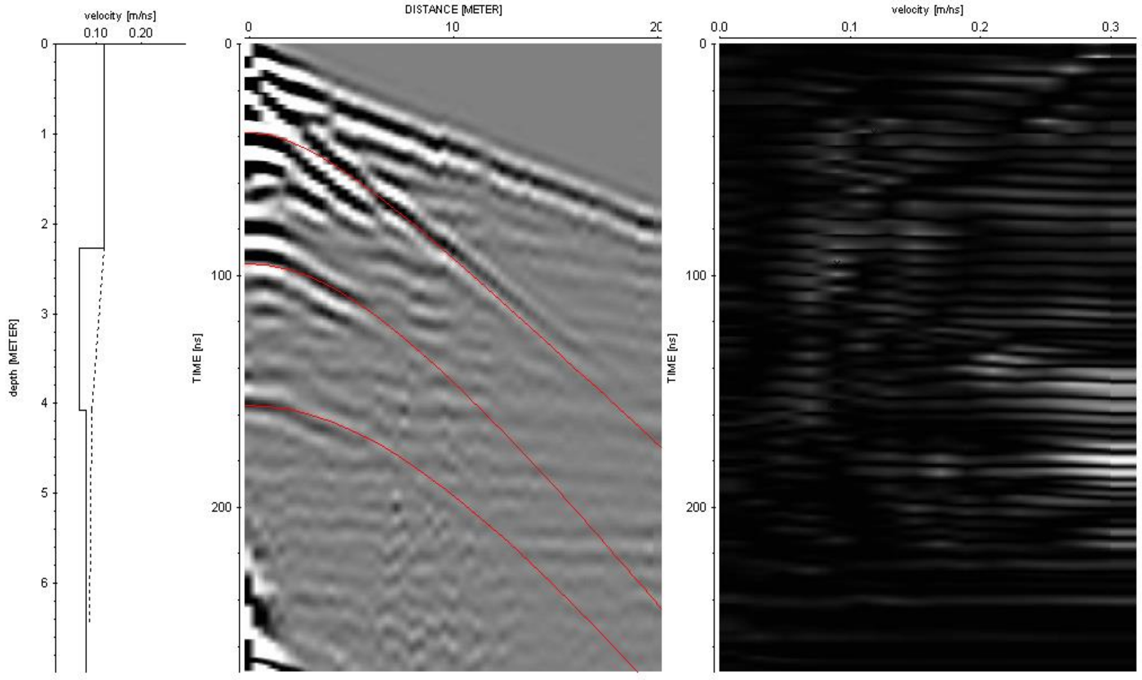

Figure 4.19. CMP measurement with 100 MHz frequency by using parallel end fire antenna orientation at the location 180 m.

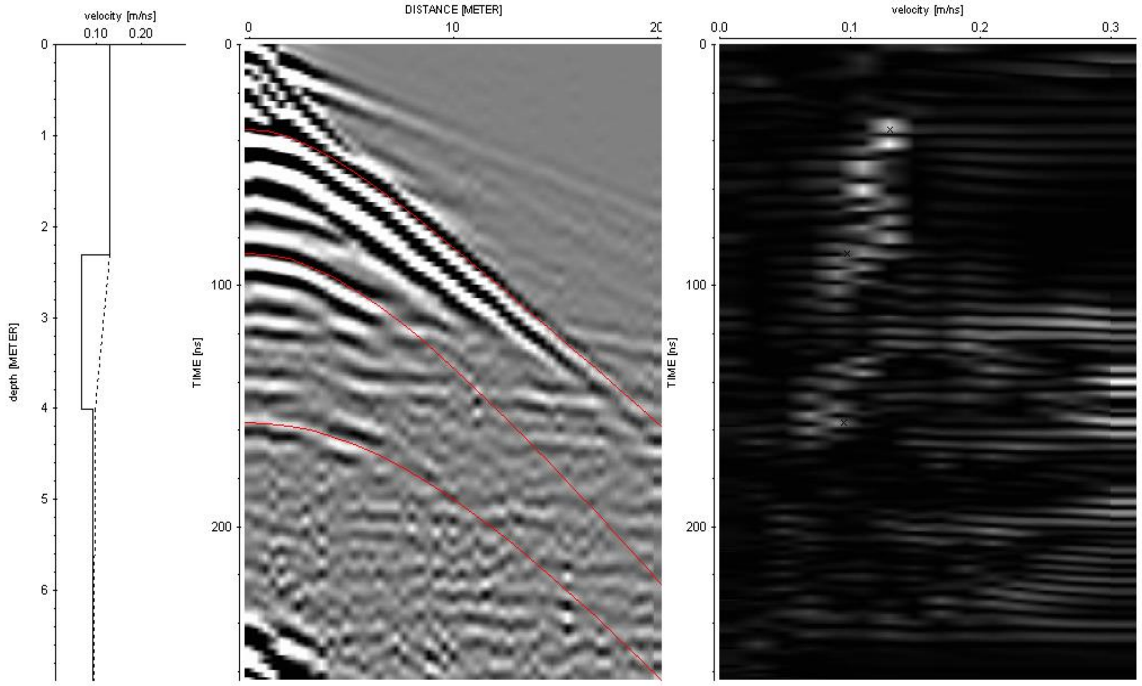

Figure 4.20. CMP measurement with 100 MHz frequency by using perpendicular broadside antenna orientation at the location 180 m.

Fig. 4.19 represents the CMP measurement with 100 MHz frequency by using parallel end fire antenna orientation. Fig 4.20 represents the complementary measurement with perpendicular broadside antenna orientation for the previous one with parallel end fire antenna orientation. At the 170 m location of the measurement 0.2 m of trace increment has beeen selected with a twenty meters of spacing. Similar procedure with the preceding measurements have been applied to collect the data at this location. They have the similar results with the measurements at 170 m point. Ground water reflections hava an evident shape at the beginning of the section. There are higher velocity reflections beneath the ground water table. Because of the intersection of ground wave and the ground water reflections at the results it was not possible to see a distinct reflection from the ground water. This problem obstructed to detect the amplitude and phase variations on the reflections. Because of this handicup it was not possible to detect the Brewster angle in this study as estimated before.

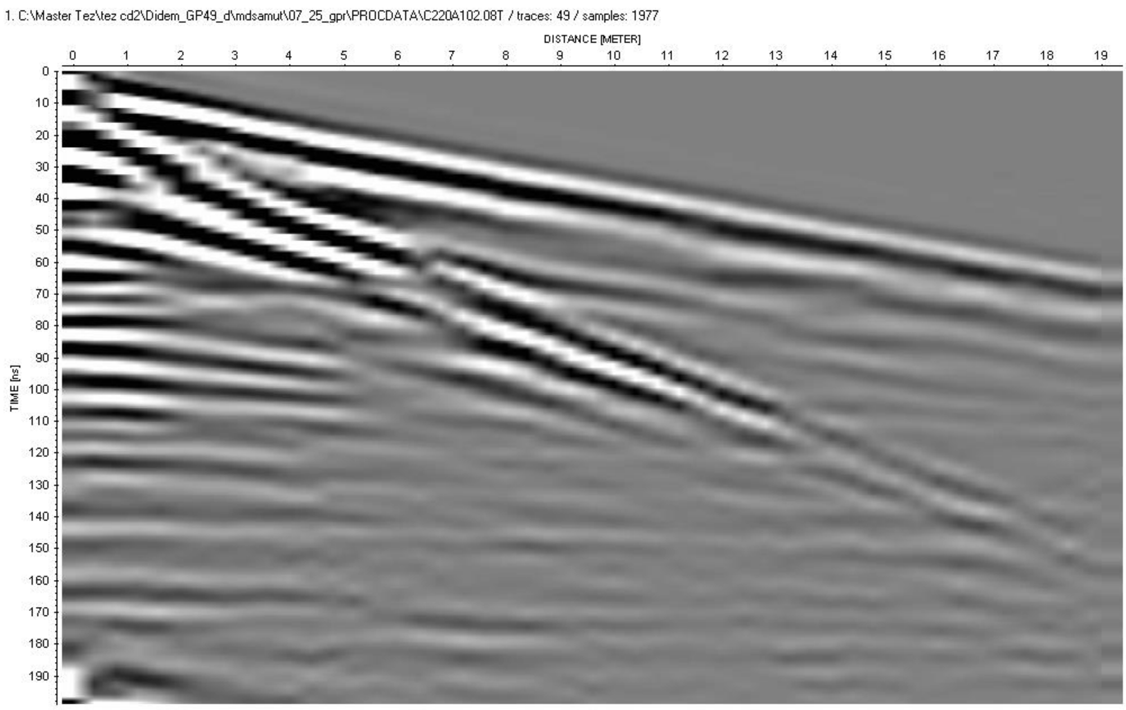

Figure 4.21. CMP measurement with 100 MHz frequency by using parallel end fire antenna orientation at the location 220 m.

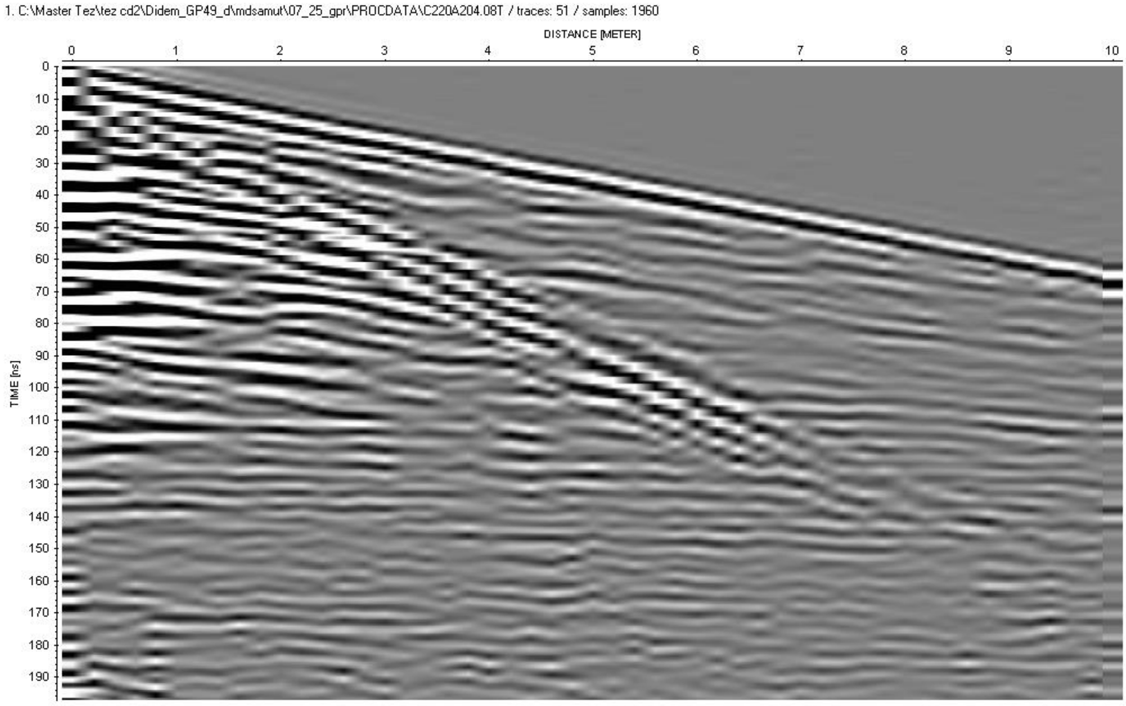

Figure 4.22. CMP measurement with 200 MHz frequency by using parallel end fire antenna orientation at the location 220 m.

Fig. 4.22 represents the CMP section from the location of 220 m as illustrated in Fig. 4.2. Application of 200 MHz frequency parallel end fire antenna orientation has been illustrated in this figure. Trace increment has been selected as 0.2 m with 20 meters of spacing. Direct air wave can be identified clearly at the top of the section. Then ground wave can be detected with the intersection of reflections from ground water. And the deeper reflections exist at the neighborhood of 90 ns. There are clearly visible phase and amplitude changes in this section. These changes cannot be dedicated to Brewster angle simply. Because of that the existence of these changes are mixing with the intersection points on the radar section. Fig. 4.22 represents the CMP section from the location of 220 m by using parallel end fire antenna orientation and 200 MHz antenna frequency. In this field measurement 0.2 m of trace increment has beeen selected with ten meters of spacing in each direction. Except the direct air wave and the ground wave, the reflections are not vlear enough to identify any small amplitude or phase change in this measurement.

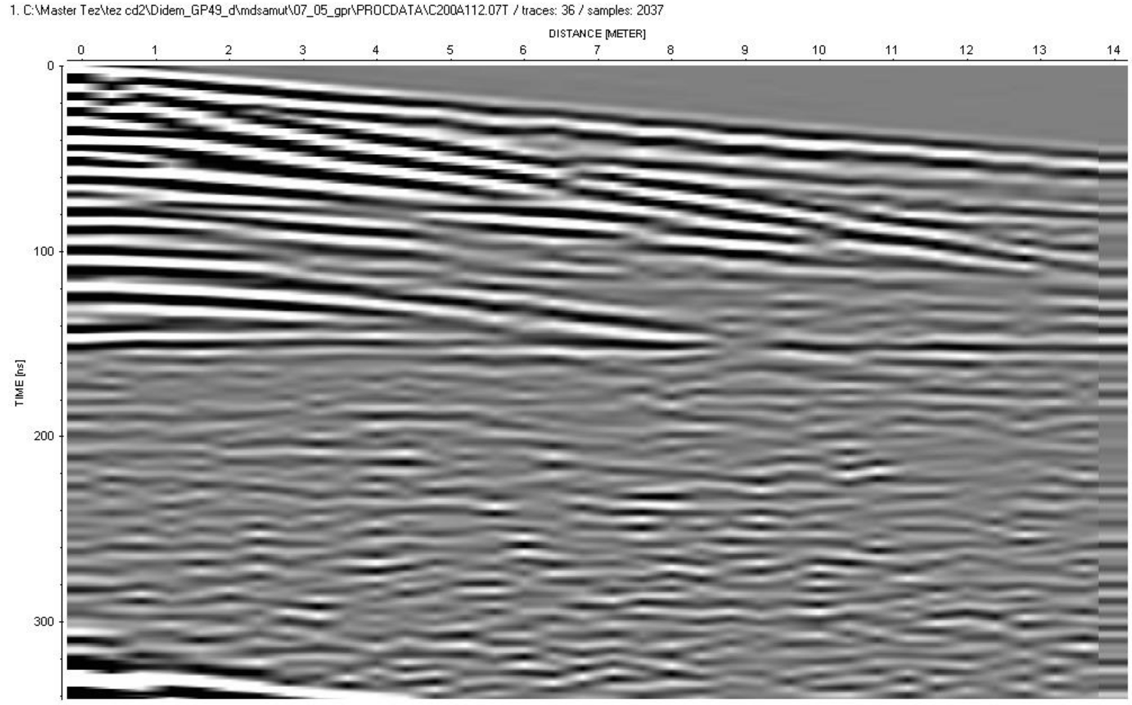

Figure 4.23. CMP measurement with 100 MHz frequency by using parallel end fire antenna orientation at the location 200 m.

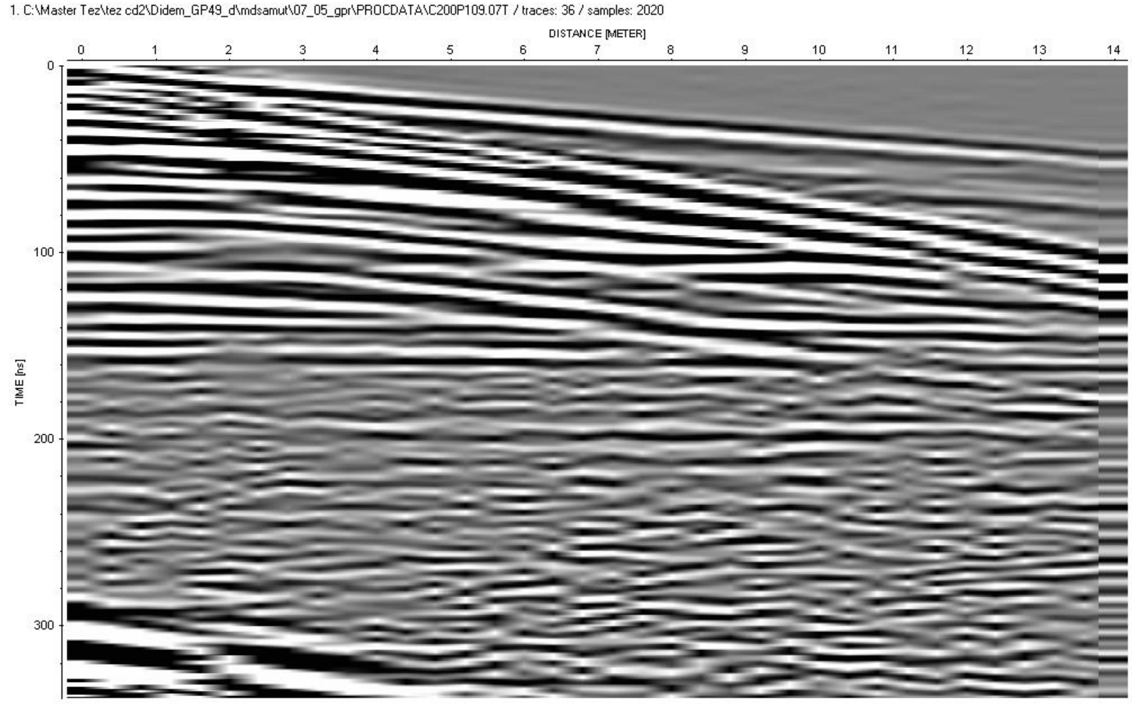

Figure 4.24. CMP measurement with 100 MHz frequency by using perpendicular broadside antenna orientation at the location 200 m.

Fig. 4.23 and Fig 4.24 represents the CMP measurements from the location of 200 m on the survey line. Fig. 4.23 is for the parallel end fire antenna orientation with 100 MHz antenna frequency and Fig.4.24 is for the perpendicular broadside antenna orientation with the same antenna frequency. Trace increment has been selected as 0.2 m. In this measurement air wave, ground wave and the reflections can be detected. There are some missing points in reflections and mixing places exist with the other waves. The strong amplitudes that exist at the upper parts of the CMP sections were caused by the high amplification of these sections.

The aim was to find the missing point in the CMP measurements caused by the Brewster angle but it is not easy in such a section to name any of the missing point as a Brewster angle. There was not use of any of the processing step such as an extensive filtering to identify these intersections. The only thing that can be done in such a situation is to refer to models. But that can just give an idea about the field conditions that from where can this angle be detected.

5. REFLECTION CHARACTERISTICS FROM THE WATER INTERFACE

5.1. Forward Modeling With REFLEX

REFLEX modeling procedure allows the interactive production of a 2-dimensional layer model and based on this layer model the simulation of the electromagnetic wave propagation by means of finite difference method. The electromagnetic simulation is based on the solution of Maxwell's equations. By doing this, it is assumed that the physical parameters ε, μ and σ are frequency independent. Electromagnetic wave propagation is simulated and stored into a wave field (x, z, t) as a function of the local coordinates and the time.

In forward modeling three different sources are supplied:

Plane wave: The plane wave can be excited in an arbitrary depth level z. It allows the simulation of zero-offset section.

Point Source: The point source can be placed at any arbitrary point in the 2-D model. So, a CMP measurement can be simulated cinematically and dynamically correct by several single experiments.

Exploding Reflector: Anew the exploding reflector model allows the simulation of a zero-offset section in a single FD simulation. Using this, it is assumed that the time t=0 for all points stemming from a reflector are the starting point of a Huygen's elementary wave.

Forward modeling have been done to compare the synthetic GPR data with the field data. Fig. 5.1 represents the forward model of the test site with the structural characteristics of the site. The electrical properties of the test site have been applied as the model parameters. Conductivity values have been adapted from the results of geoelectric measurements that have been carried out at the same field. Dielectric constant values have been determined from the samples. Magnetic permeability values have been taken as 1, which is appropriate for most of the subsurface materials. Source type, boundary conditions, frequency and the positions of the transmitter and receiver antennas can be selected as desired in the forward modeling with REFLEX. Processing steps can be also applied to the synthetic GPR data.

Aim of this study was to investigate the reflection coefficient characteristics with respect to different antenna orientations. So, forward modeling have been done with different antenna orientations to compare the results with the measured data from the test field. Fig. 5.1 illustrates the modeled data for the test field with transmitter and receiver antennas located parallel to the profile direction. Air wave can be detected easily at the top of the section. Reflections from the dielectric contrasts can be detected after the direct air wave arrivals. But to distinguish the reflections is not easy because of the overlay of the ground wave. Similar problem with the measured data occurs at the synthetic data. The reflections from the dielectric contrasts, mixed with the ground wave.

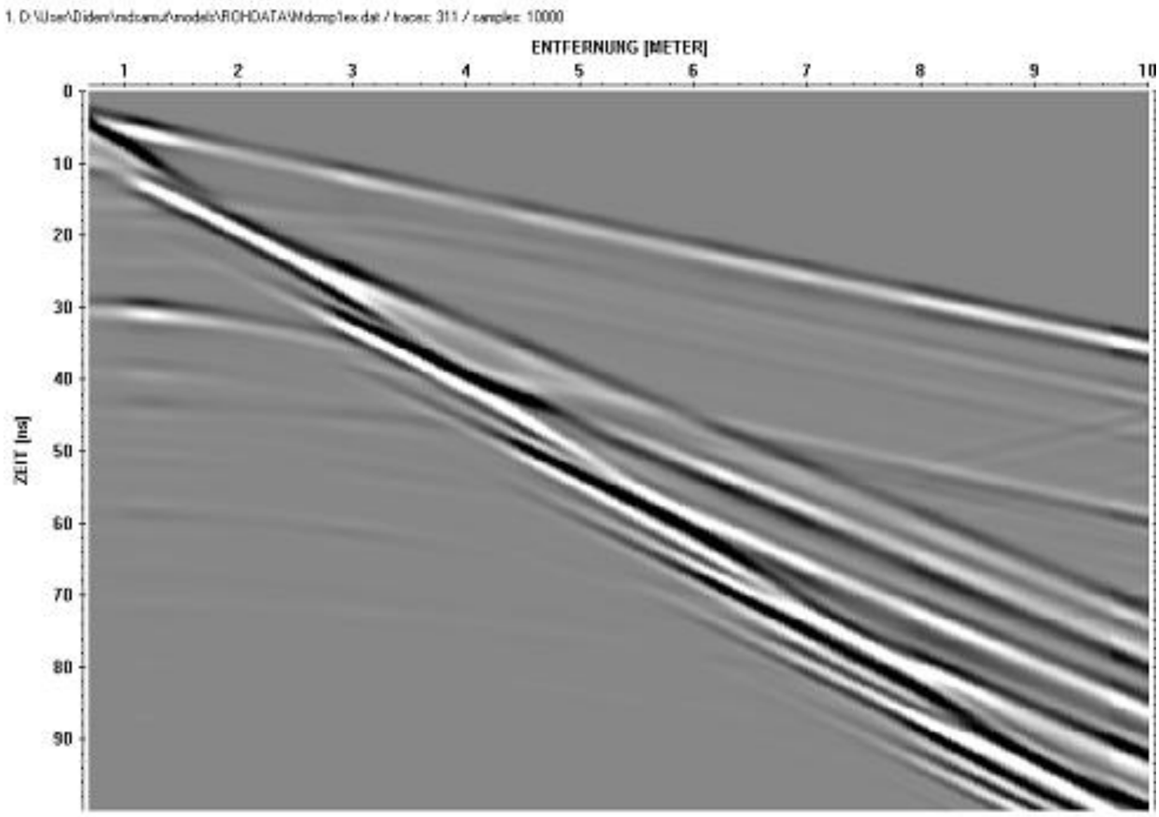

Figure 5.1. Presented synthetic GPR data modeled for antenna orientation parallel to the profile direction.

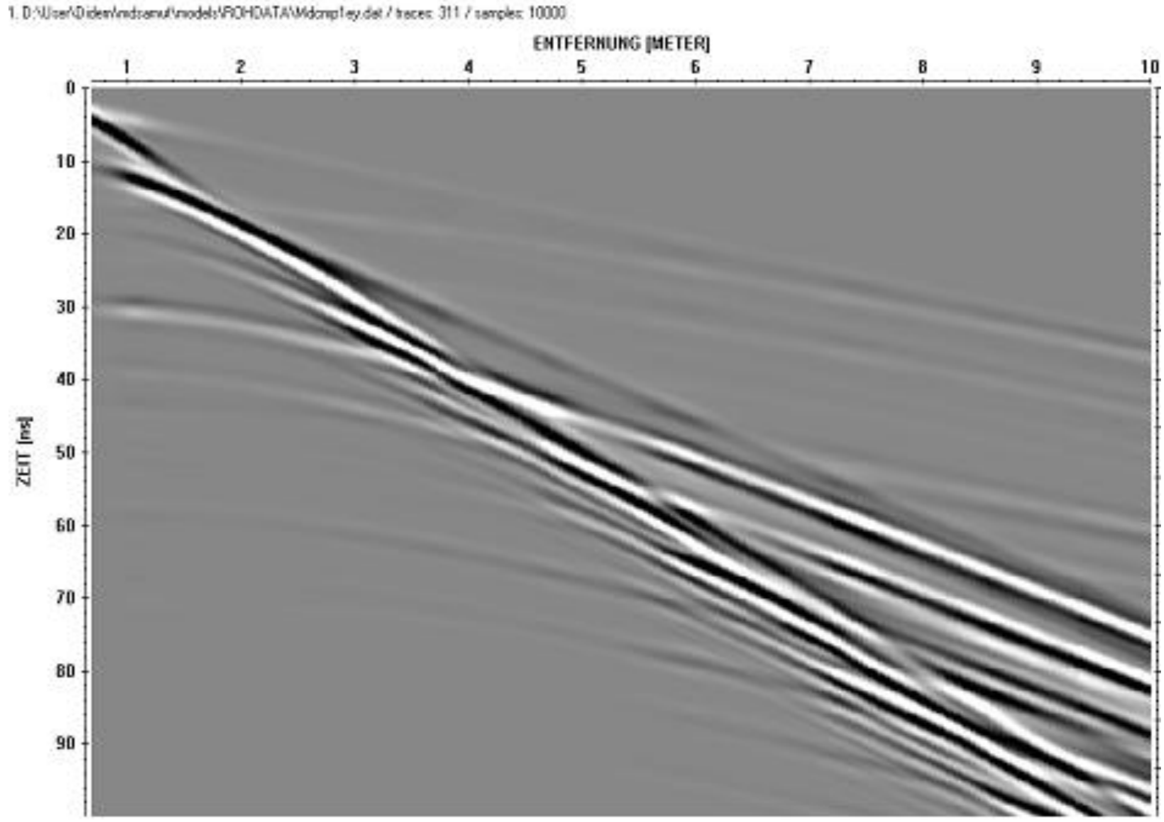

Figure 5.2. Presented synthetic GPR data modeled for antenna orientation perpendicular to the profile direction.

Fig. 5.2 illustrates the model with transmitter and receiver antennas located perpendicular to the profile direction. As expected to be, it is not different from the synthetic data obtained with other antenna orientations as represented in Fig. 5.2. Air wave, ground wave and the other reflections can be detected. But the amplitudes of the waves getting differ from the one in Fig. 5.1. At the first model with the one, in which the antenna orientation is parallel to the profile direction, we expect to see the Brewster angle. But because of the intersection of ground wave with other reflections, overlay at a point, so it is not possible to identify what is happening at that point. And it is not possible to detect any phase change or amplitude variation. But it is clear to identify the amplitude variations in the reflection from ground water at the Fig.5.1 up to 3rd meter where the wave intersects with ground wave and other reflections. These strong amplitude variations can't be seen in Fig. 5.2. Because of the characteristics of this test site, it was not possible to detect any variation in the name of Brewster angle.

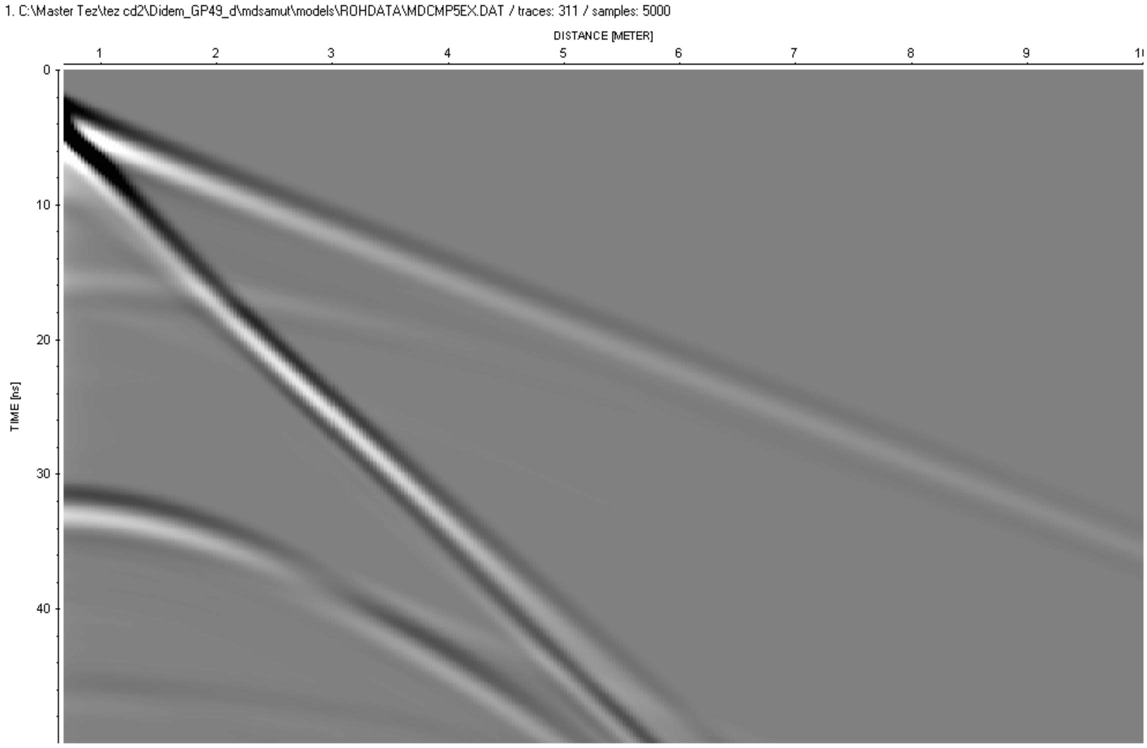

Figure 5.3. Presented synthetic GPR data modeled for antenna orientation parallel to the profile direction.

It is clear that the abundance of ground water at very shallow depth obstruct to identify individual reflections from the underground structures. So it can be fruitful to model a deeper ground water to detect the reflections without an intersection with the other waves. For this aim a new model has been constructed for a deeper ground water at the subsurface. Fig. 5.3 represents a new forward model by using similar model parameters. Parallel antenna orientation to the profile direction has been selected in the model. The depth of the ground water has been increased and the time window also diminished to decrease the processing time in the presented model. Now it is obvious that this model gives more clear results to detect the reflected waves individually. With the increase in depth of water table, it was possible to obtain distinct ground wave and ground water reflections, in the new model. Now air wave, ground wave and reflections can be detected separately. Intersection of ground wave and the other reflections does not obstruct the determination of amplitude and phase variations at the reflected waves. Amplitude variation with a change in phase at the same location can be detected clearly.

5.2. Reflection Coefficient Characteristics

Reflection coefficient characteristics of an electomagnetic wave at an interface can be determined by the equations Eq. 2.30 and 2.31 for the TE and TM modes, respectively in a perfect dielectric media. A MATLAB program called RKK were used to calculate the reflection coefficient characteristics which is written by A. Helm.[18] Calculated reflection coefficient characteristics by using this MATLAB file allow to study the behavior of amplitude and phase of the EM waves reflected from a boundary with different electrical properties. These electrical properties such as conductivity magnetic permeability and dielectrical permittivity, used as the parameters of this program. Magnetic permeability of the medium is accepted as 1, which can be used for most of the geological materials. Dielectrical permittivity and the conductivity of of two different media are the input values of this program. With these parameters, it calculates the reflection coefficient characteristics of the interface and constitutes the resultant graphic.

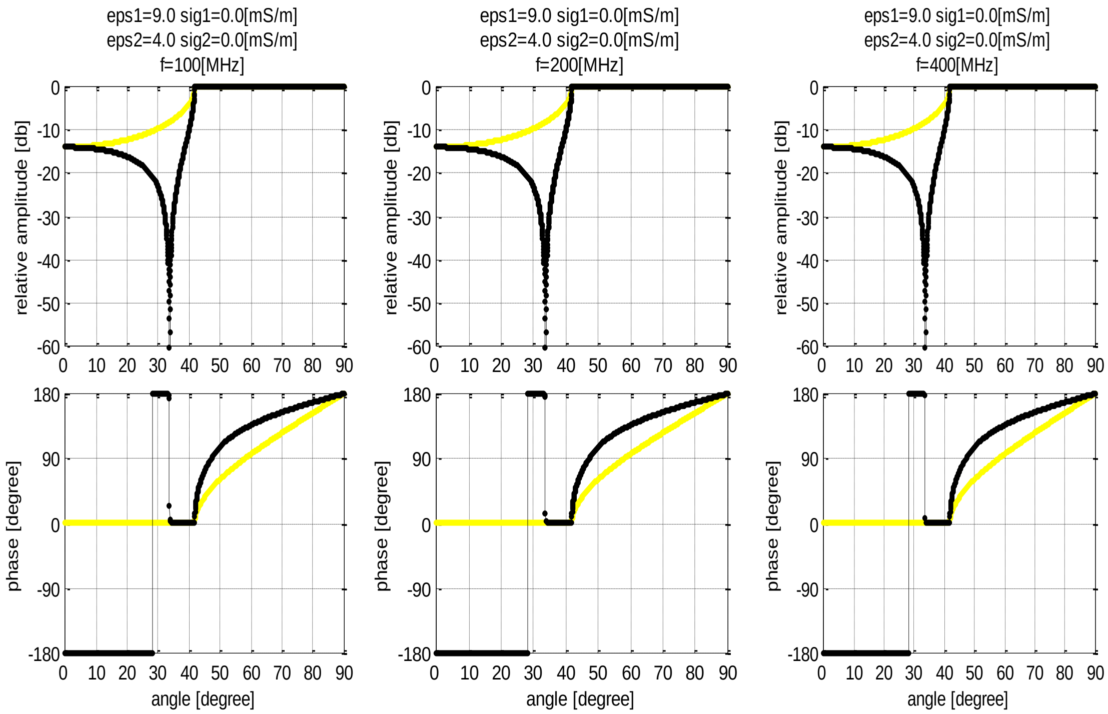

Figure 5.4. Humus-sand interface calculated with 100 MHz, 200 MHz and 400MHz frequencies.

The yellow line represents the reflection coefficient for the antenna orientation perpendicular to the profile direction. Black line is for the parallel orientation. The angle under which the amplitude decreases abruptly, represents the Brewster angle. Fig. 5.1. and 5.2. represents the examples of reflection coefficient calculation. According to the field characteristics, the first interface at the test field was the humus sand interface at a depth of 0.4 m. Fig. 5.1 represents the reflection coefficient characteristics for humus sand interface. Resultant graphics state the responses for 100 MHz, 200 MHz and 400 MHz frequencies from left to right, respectively. It can be seen from each figure that the relative amplitude values has an abrupt decrease at an angle of $\cong$ 33 degrees. At the same point, phase change can be also identified. This angle, under which the amplitude decresases very strongly, can be reffered as the Brewster angle. This phenomenna just occurs in parallel antenna orientation with the parallel antenna orientation. The perpendicular orientation which is represented as a grey line does not has any abrupt change in amplitude. The phase of the perpendicular orientation has a change at this point but it is not sharp as the parallel orientation. This variation in phase and amplitude depends on the conductivity and dielectrical properties of the medium. If the medium is not conductive, this change in amplitude occurs strongly, but with increasing conductivity the break-down weakens itself.

The interface of sand with water saturated sand exists beneath the humus sand interface. Fig. 5.2 illustrates the reflection coefficient characteristcis from sand to wet sand. Dielectric permittivity values for this interface is accepted as 4 to 25, respectively. Conductivity values for this interface was taken as 0.01 mS/m to 1 mS/m. The sharp relative amplitude variation will be observed at nearly 69 degrees for parallel antenna orientation. And the phase change for parallel antenna orientation will occur at the same point. These angles can be determined from the sine and cosine ratios where these variations observed. The problem in the real field data was the difficulty in identification of Brewster angle because of the field characteristics. In this test field the ground water was at a depth of approximately two meters. At this depth, the reflections from the ground water intersect with the ground wave. So, it was not possible to detect the change in amplitudes and phases of the waves at this point.

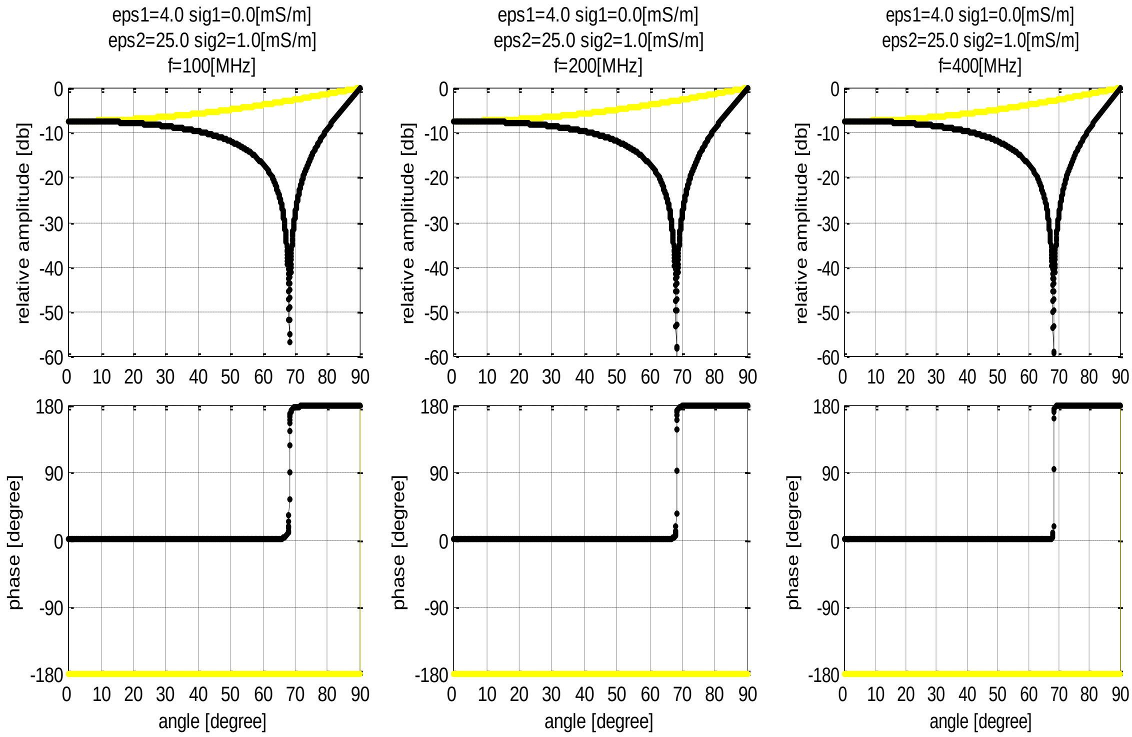

Figure 5.5. Sand-saturated sand interface calculated with 100 MHz, 200 MHz and 400MHz frequencies.

5.3 Antenna Characteristics

The aim of this present work was to investigate the Brewster angle to determine the dielectric permittivity of the second medium. For this object, amplitude losses in radar measurements was searched to determine this angle. But the amplitude loss in a radar measurement does not occur with only the existence of Brewster angle. Antenna directivity cause the same effect, amplitude loss in radar waves, because of its strong directivity pattern. When the researcher faced with a strong amplitude loss in a GPR measurement, he must not consider it directly as a Brewster angle. Amplitude loss in measurements may be either a Brewster angle or an antenna radiation property. So, it must be discussed that the Brewster angle not only exists with an amplitude loss but also with a phase change of 180 degrees. The advantage of searching antenna charateristics to distinguish it from Brewster angle is that the antenna characteristics not display a phase change with amplitude loss.

In the previous division, amplitude and phase variations have been discussed, which is used to determine the Brewster angle. Dipole antennas were used in most of the GPR equipment as the transmitting and receiving antennas. These antennas show strong radiation characteristics. These radiation characteristics of a dipole antenna for parallel and perpendicular antenna orientation has been studied by using a MATLAB program which is written by A Helm [17]. According to the directivity phenomena of the dipole antenna the radiated energy does not travel with same energy at the subsurface. Fig. 5.6 llustrates the radiation pattern of a dipole antenna for air-earth interface. According to this illustration it is expected that at some locations in the measurements, there must be some weak energy distrubution because of the antenna characteristics. The location of this weak energy distribution in measurements can be determined by forward modeling of antenna characteristics. These locations can be distinguished from the amplitude losses caused by the existance of Brewster angle at a point.

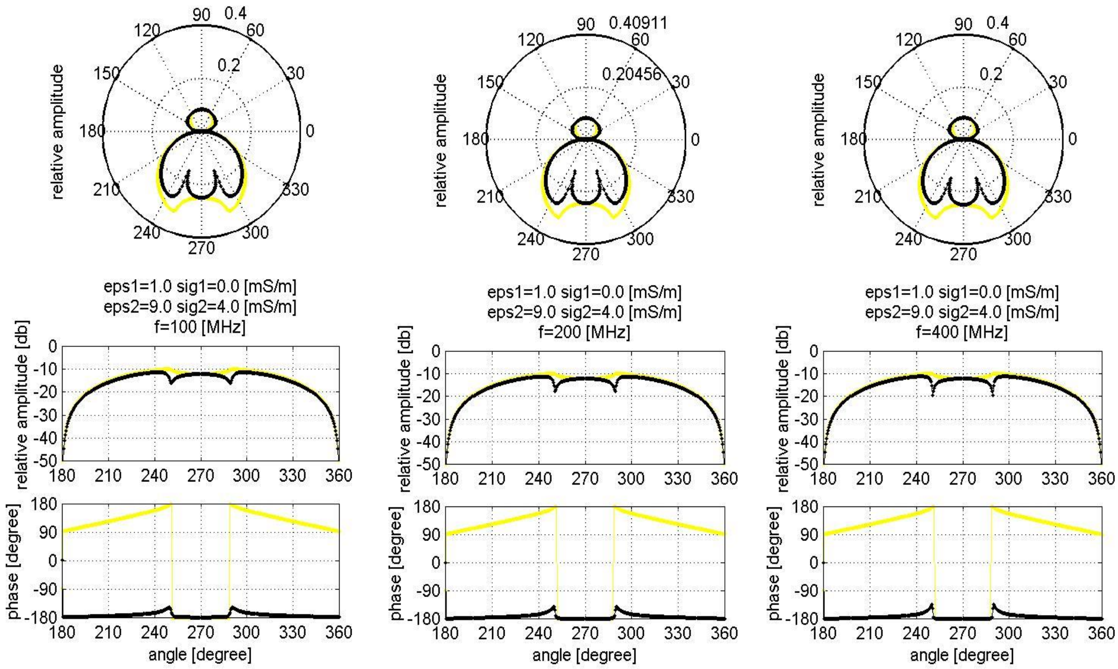

Figure 5.6. Air-humus interface modeled for 100 MHz, 200 MHz and 400MHz frequencies.

In Fig. 5.6 Air humus interface have been modeled for 100MHz, 200MHz and 400 MHz frequencies. Dielectric constant and conductivity values taken as 1 and 0 mS/m for air and 9 and 4 mS/m for humus, respectively. Radiation characteristics of two antenna orientations at an interface are particularly different. Antenna directivity pattern for a parallel orientation demonstrates a three-lobed structure with sharp nulls in the radiation and a scalloped two lobe structure for the perpendicular antenna orientation. The yellow line represents the antenna characteristics for perpendicular antenna orientation and black line represents the parallel antenna orientation. It can be realized on Fig. 5.6 that the relative amplitude variations occur at two points which exists at similar locations for both antenna orientations at an angle of approximately 21 degrees. Phase change does not occur for parallel antenna orientation. This is the point that the results can be distinguished from the reflection coefficient characteristics. Phase change for perpendicular antenna orientation can be detected more clear than the parallel orientation. Three different frequency results state that the antenna characteristics do not change by antenna frequency. Amplitude and phase characteristics remain the same for all frequencies.

5.4. Comparison And Results

Reflection characteristics from the water interface can be examined by a number of different ways. Forward modeling with the radar software, reflection coefficient characteristics modeling are some of the examples for this. Results of these detailed examination can utilize the determination of Brewster angle. Detection of Brewster angle in radar measurements allow to identify the dielectric permittivity ratios for that interface. This information help to identify the characteistics of unknown second layer at that interface. Ground water is the most important layer in this study. The aim of the field measurements were to obtain the amplitude loss and phase variations together from ground water reflections to detect the material charactersitics under this water saturated layer. Unfortunately, this was not possible for the field of this subject in Tiergarten. In this area water intrusion has a depth of approximately two meters beneath the humus and sand layers. This water intrusion was so shallow that the reflections from this dielectric contrast intersect with the ground wave which also exists in the beginning of the radar sections. In forward models of field parameters the resultant section has the same result with the measured data. Water reflectionsoverlay with the ground wave after a few ns from the beginning. This obstruct to search amplitude variations and phase change in the reflections. Fig. 5.3 represents a good example for existence of Brewster angle. In this example water intrusion modeled with a deeper depth to compare it with the original field model. In this model redlections from ground water can be identified clearly. Amplitude loss and the phase variations are obvious in this reflections which are seperated from the other waves.

Reflection coefficient characteistics of interfaces can be studied with forward modeling. In the second part of this chapter reflection coefficient characteristics at an interface has been discussed. According to the explained models in this subchapter, location of the Brewster angle can be studied according to the physical properties of the interface. Examples represent existence of Brewster ange at different interfaces. According to the Fig. 5.3 if there is an interface of humus – sand with dielectric permittivities of 9 to 4 respectively, the Brewster angle is expected to see at angle of ≅ 33 degrees fro this interface. These examples can be increased according to desired electrical parameters. With the help of this work we can have a preview for the wave behavior.

Antenna characteristics can be searched with a similar method. Radar system has a strong directivity because of the dipole antenna that it use. Radiation characteristics can be modeled for the desired interface, for instance air-earth interface, as in Fig. 5.6. This gives a knowledge about the radiated energy into the subsurface. These antenna characteristics also depends on the antenna orientation as the reflection coefficient characteristics. Parallel antenna orientation and perpendicular antenna orientation according to the survey line have different antenna and reflection coefficient characterictics. Knowledge of the energy losses due to the antenna characteristics can be helpful in determining these effects in radar sections. Amplitude variations in signal can be also seperated from the one, caused with the existence of Brewster angle at that location.

In a field survey with ground penetrating radar, if the aim is to detect the Brewster angle, a couple of things can be done. First of all, radar measurements must be examined in detail to detect the Brewster angle. In any amplitude loss and phase change, it must be thought twice to assign this as a Brewster angle. An amplitude loss in radar measurements can be caused by the existence of the Brewster angle or the antenna characteristics. It is already known that no phase change exists due to the antenna characteristics. So, this property can be a way to differentiate changes due to the Brewster angle from the ones caused by antenna characteristics. The other way is to locate the amplitude losses due to the antenna characteristics and differentiate these locations from the locations that Brewster angle exists. Forward modeling with Reflex can also provide fruitful information in determination of Brewster angle. The results of these models can be compared with the other characteristics for further information.

6. SUMMARY AND CONCLUSIONS

In this present work GPR measurements were performed to determine the reflection coefficient characteristics with different antenna orientations. The aim of this present work was to investigate the reflection coefficient characteristics with different antenna orientation at a test field above the ground water. Detection of Brewster angle in CMP measurements was another subject of this thesis to study. The main orientations used in this work are the ones with the electric field, perpendicular and parallel to the plane of incidence. Brewster Angle can be detected on CMP measurements with antenna orientation that the electric field is parallel to the plane of incidence. The existence of Brewster angle in radar measurements, provide useful information on determination of the dielectric permittivity of the unknown layer beneath the interface. For this purpose, parallel and perpendicular antenna orientations to the profiling direction have been used for variable offset and constant offset measurements by using 50, 100, 200, 400 MHz antenna frequencies, in the selected field. More than 150 profiles were carried out and all the data have been processed, interpreted and then compared with different orientations.

Most important result of the constant offset measurements was the dependency of radar data to the antenna orientation. A variety of antenna orientation has been used at the same field to detect the reflection characteristics. Results state that different antenna orientation may give different responses to the subsurface structure. Some of the subsurface structures can be detected with an antenna orientation but cannot with another. This event reveals that the optimum antenna orientation must be selected in radar surveys. The antenna orientation can be selected after a number of test measurements in the investigated field. Use of various orientations in radar measurements will provide more reliable results.

One of the other subject to study in this thesis was to detect the Brewster angle in CMP measurements with parallel end fire antenna orientation. For this purpose, CMP measurements have been collected to investigate the Brewster angle. In this test field, the ground water exists at a depth of approximately two meters. The reflections from this ground water were intersecting with the ground wave because of the shallow depth of ground water. This overlay of waves, which is caused by the subsurface characteristic, obstructed the detection of Brewster angle at the radar sections. Because of this reason, it was not possible to identify the Brewster angle.

In order to study the Brewster angle, reflection characteristics from ground water has been discussed. Forward model for the field has been obtained with the test field's electrical parameters. Results show that the field data is in good agreement with the modeled synthetic data. Another model has been developed with forward modeling manual to see the existence of Brewster angle. Reflection coefficient characteristics and antenna characteristics also studied with the field parameters. Amplitude variations and phase changes due to the Brewster angle existence can be examined with reflection coefficient characteristics. Investigation of antenna characteristics can be utilized to ensure the existence of Brewster angle in radar measurements.

REFERENCES

[1] **Stratton, J. A.,** 1941. Electromagnetic theory, McGraw-Hill, New York,

[2] **Ward, S. H. and Hohman, G.W.,** 1988. Electromagnetic Theory for Geophysical Applications, 1, pp. 131-312, II, Soc. Exp. Geophys. Tulsa, Oklohama

[3] **Telford, W., M., Geldart, L. P. and Sheriff, R. E.,** 1990. Applied geophysics, University Press, Cambridge

[4] **Sharma, P. V.,** 1997, Environmental and engineering geophysics, University Press, Cambridge

[5] **Reynolds, J. M.,** 1997. An Introduction to Applied and Environmental Geophysics, John Wiley Sons, 1997

[6] **Annan A. P. and Davis, J. L.,** 1989. Ground-Penetrating Radar for high – resolution mapping of soil and rock stratigraphy, *Geophysical Prospecting*, **37**, 531-551

[7] **Topp, G. C., Davis, J. L. and Annan A. P.,** 1980. Electromagnetic determination of soil water content: Meausrement in coaxial transmission lines. *Water Resources Research*, **16**, 574-582

[8] **Timothy, B.,** 1994. Antenna design, University of Colorado, Boulder,

[9] **Jasik, H.,** 1961. Antenna engineering handbook, McGraw-Hill New York,

[10] **Arcone S. A.,** 1995. Numerical studies of the radiation patterns of resistively loaded dipoles, *Journal of Applied Geop*, **33**, 39-52

[11] **Du, S.,** 1996. Determination of water content in the subsurface with GPR, *PhD Thesis,* Munich University, Germany

[12] **Müller, M., Mohnke, O., Schmalholz. J. and Yaramancı U.,** 2002. Interurban – Geophysical assessment of water dynamics and solute transport in urban soils. Berlin Technical University.

[13] **Assmann, P., and Gandert, G.,** 1957. Der geologische Aufbau der Gegend von Berlin. Heraus gegeben vom Senator für Bau und Wohnungswesen.

[14] **Parasnis, D. S.,** Principles of applied geophysics, pp 246-262 Chapmann & Hall, 1997

[15] **Cai, J., and McMechan, A.,** 1995, Ray-based synthesis of bistatic ground – penetrating radar profiles. *Geophysics*, **60**, 87-96

[16] **Annan, A., P.,** Practical processing of GPR data. Sensors & Software Inc. Missisauga, Ontario

[17] **Yılmaz, Ö.,** 1988. Seiscmic data processing, Soc. Expl. Geophysics, Tulsa

[18] **Helm, A.,** 1998. Einfluss von Offset und Antennaorientierung auf Reflexionsmerkmale beim Bodenradar, *Diplomarbeit*, Berlin Technical University, Germany

CURRICULUM VITAE

Musavver Didem Samut was born in 15 March 1978, in Izmir. After graduating from Burak Bora Anatolian High School she has began to study Geophysical Engineering in Istanbul Technical University in 1997. She’s got a Bachelor of Science degree in 2001 with honor degree in Geophysical Engineering Department. In September 2001 she started her M.Sc. in the same department of the same university where she is still continuing her studies.